

Daniel Scheiber

Ab initio calculation of small silver clusters

Masterarbeit

zur Erlangung des akademischen Grades eines Magisters

an der Naturwissenschaftlichen Fakultät der

Karl-Franzens-Universität Graz

Betreuer:

Ass.-Prof. Dr. Peter Puschnig

Ao. Univ. Prof. Mag. Dr. Ulrich Hohenester

Institut für Physik

Fachbereich für Theoretische Physik

2013

Abstract

This thesis is concerned with the calculation of the structure and the optical properties of small silver clusters (Ag_1 to Ag_5) with a special focus on Ag_3 . For the calculations of the structure and the electronic spectra I am applying Density Functional Theory and its time-dependent expansion within the Casida formalism, that is implemented in the program package ABINIT. Next I am comparing the calculated spectra to experimental data from literature.

Further, I am investigating the vibronic transitions of an electronic excitation for Ag_3 using the Franck-Condon principle. In doing so I am also looking into the temperature dependence of vibronic transitions.

Contents

1	Introduction	1
2	Basics	3
2.1	Atoms and Molecules	4
2.2	Lagrange and Hamilton formalism	6
2.2.1	Lagrange formalism	6
2.2.2	Hamilton formalism	8
2.3	Schrödinger equation	10
2.4	Franck-Condon principle	12
3	Theory	14
3.1	Density Functional Theory	16
3.2	Time dependent Density Functional Theory	20
3.2.1	Casida formalism	21
4	Results	24
4.1	Convergence Parameters	25
4.2	Structures for the clusters Ag_2 to Ag_5	31
4.2.1	Ag_2	31
4.2.2	Ag_3	31
4.2.3	Comparison	36
4.3	Optical spectra for the clusters Ag_2 to Ag_5	38
4.3.1	Ag_3 spectrum	42
4.4	Vibronic energies for Ag_3	46
5	Conclusion	52
	Acknowledgements	53
	Used Software	54

AB INITIO CALCULATION OF SMALL SILVER CLUSTERS

Contents

Bibliography

55

1 Introduction

Starting with birth human beings are driven by curiosity. How does the world around us function? What is it made of? Science gives us a lot of answers to our questions and additionally raises new interesting questions. In order to provide these answers, scientists all over the world have always tried to look deeper into the matter around us. Especially since the last century it is possible to investigate and work with smaller particles than ever before. An interesting branch of these discoveries is nanotechnology, which also introduces nanoclusters, that are especially important for this work.

One feature of those nanoclusters, not totally understood by now, is that

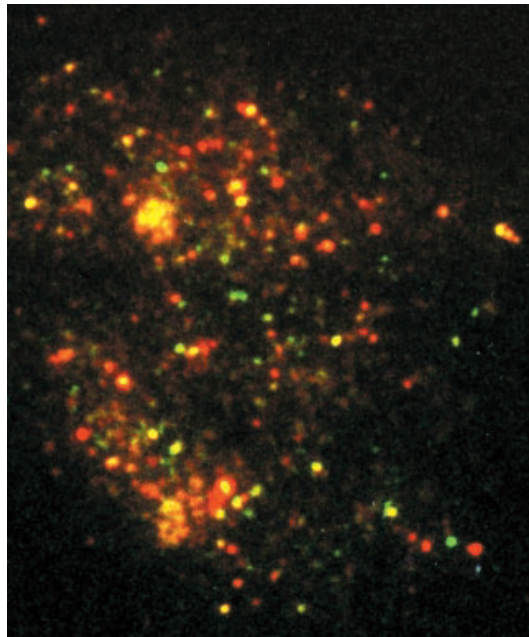


Figure 1.1: Picture of fluorescence from a 16.6-nm Ag/Ag₂O film excited at 514.5 nm, taken from [1].

small silver clusters show strong photo activated emission for short wavelengths ($\lambda < 520$ nm). What is even more interesting is the fact, that the clusters blink

AB INITIO CALCULATION OF SMALL SILVER CLUSTERS

1 Introduction

and change their emission wave length [1]. Figure 1.1 shows a picture of fluorescent silver nanoclusters of different sizes emitting at different wave lengths. The aim of this work is the ab-initio calculation of the absorption spectra of different small silver clusters within the framework of density functional theory. With that at hand, it may be possible to tell which wavelengths are emitted from which cluster.

Some literature already exists on these problems: calculations of the structure and the absorption spectra of small silver clusters have been done in [2, 3, 4, 5, 6], some of these will later on be used for comparison with the computed results. From the experimental section literature on measurements of structures, emission and absorption spectra can be found in [1, 7, 8, 9, 10]. Throughout this work, if not especially mentioned otherwise, atomic units are used. This unit system is very convenient in atomic and molecular physics, as some of the most used units are set to unity. These units and units derived from them are given in Table 1.1.

Table 1.1: Atomic units ($m_e = 1/(4\pi\epsilon_0) = e = \hbar = 1$) and quantities derived from them (E_h and a_0).

Quantity	Name	Symbol	SI units
Mass	electron rest mass	m_e	$9.109 \cdot 10^{-31}$ kg
Length	Bohr radius	a_0	$5.292 \cdot 10^{-11}$ m
Charge	elementary charge	e	$1.602 \cdot 10^{-19}$ C
Angular momentum	reduced Planck's constant	\hbar	$1.054 \cdot 10^{-34}$ Js
Energy	Hartree energy	E_h	$4.360 \cdot 10^{-18}$ J
Electrostatic constant	Coulomb's constant	$1/(4\pi\epsilon_0)$	$8.988 \cdot 10^9$ N m ² /C ²

2 Basics

This chapter deals with some fundamental knowledge needed to follow this work. The first section contains some facts about atoms and molecules, what holds them together and what they consist of. Also the foundation of their mathematical description, the Schrödinger equation, will be summarized shortly. The Lagrange formalism and the Hamilton formalism are used later in this work and a short section deals with the basic framework of these two methods. The last section of this chapter discusses the Franck-Condon principle in molecules and its consequences.

2.1 Atoms and Molecules

All matter around us is made of atoms. We ourselves are made of atoms. This has been postulated long time ago, as records of ancient Greeks and other philosophers tell us. The development of a better model of the atom has thrived at the beginning of the 20th century. Different atom models have been published and discussed until the theory of quantum mechanics has been well-established. Thereby also the idea of the indivisibility of atoms had to be abandoned.

The atom consists of protons, neutrons and electrons. While the protons and the neutrons are located in the center of the atom, the electrons build a negative charge cloud around the nucleus. The nucleus is built of the positive charged protons and the charge neutral neutrons. They stick together due to the strong nuclear force. The electrons are hold in place by the Coulomb force. The number of protons in the nucleus is called atomic number and specifies the element. On Earth 94 different elements can be found, more have been synthesized. For Silver (Ag) the atomic number is 47. This tells us that one neutral silver atom consists of 47 protons and as many electrons. The sizes of atoms range from $1 \cdot 10^{-10} - 3 \cdot 10^{-10}$ meters, while the nuclei themselves are much smaller with sizes in the range of $1 \cdot 10^{-15} - 5 \cdot 10^{-15}$ meters. Each of this atoms has characteristic chemical properties defined by the number of protons, neutrons and electrons it is made of.

The different atoms do not only exist independently, they interact with each other and form clusters and molecules consisting of atoms of the same kind or a mixture of atoms. The smallest molecules are assembled by just two atoms, for example N_2 or H_2 . Larger molecules can be proteins or nucleic acids like the DNA. The atoms within molecules bind together because of chemical bonds between the atoms. The properties of molecules can be very different from the atoms they consist of and depend upon the atoms they are made of, the structure and the way in which the atoms are arranged in the molecule, binding energies of the atoms and the energy required to change the structure of the molecule [11].

2 Basics

In which way atoms and molecules and their interaction are described depends upon the problem in question. For some problems it is sufficient to just look upon the valence electrons, for other problems additionally the core electrons of the atom have to be taken into account. To treat molecular vibrations of a molecule, partly Newtonian mechanics can be used and the atoms are modelled as points in space, located at the center of mass of the atom. In that way Ag_3 will be treated in Section 4.4 to extract the vibronic transitions of the cluster.

2.2 Lagrange and Hamilton formalism

2.2.1 Lagrange formalism

The Lagrange formalism is a very powerful tool in classical mechanics. The formalism allows in general to solve complex systems with a minimum amount of work. It can be understood as a generalization of the principles of classical mechanics, i.e. Newton's axioms. Contrary to the Newton axioms, the Lagrange formalism makes it possible to take constraints to a problem easily into account. The formalism is embodied either in the Lagrange equations of the first kind, including constraints by additional constraint equations, or in the Lagrange equations of the second kind, incorporating the constraints with generalized coordinates.

The Lagrange equations of the first kind are given as [12]:

$$m_n \ddot{r}_n = F_n + \sum_{\alpha=1}^R \lambda_{\alpha} \frac{\partial g_{\alpha}(r_1, \dots, r_{3N}, t)}{\partial r_n} \quad n = 1, 2, \dots, 3N \quad (2.1)$$

$$g_{\alpha}(r_1, \dots, r_{3N}, t) = 0 \quad \alpha = 1, 2, \dots, R$$

The sum runs over all R constraints and there are, all together, $3N$ differential equations and R constraint equations. As can be seen in equation (2.1), the Lagrange equations of the first kind are an extension to the Newtonian equations of motion extended by the constraint forces. A constraint equation of the form $g(r_1, \dots, r_{3N}) = 0$ is called holonomic. These holonomic constraint equations significantly simplify a problem, because they reduce the degrees of freedom of a problem by R .

Usually it is not necessary to know the exact form of the constraint forces. The Lagrange equations of the second kind offer an even more elegant way to derive the equations of motion for the system in question. The system is described by generalized coordinates, which are any coordinates (q_1, q_2, \dots, q_f) , that completely define a system of f degrees of freedom [13]. So the $3N$ coordinates $\{r_i\}$ reduce to $3N - R = f$ generalized coordinates $\{q_j\}$, that automatically satisfy

2 *Basics*

the holonomic constrained equations. A typical example would be a simple pendulum in two dimensions with mass M , the movement of the pendulum is constrained by the rod of length l to a circle. The system can be described, for instance, with Cartesian coordinates $\{x_1, x_2\}$ and the constrained equation

$$x_1^2 + x_2^2 - l^2 = 0. \quad (2.2)$$

Because the movement is constraint from the two dimensional plane to a one dimensional curve, the degrees of freedom for the system are just one, hence it is possible to define a generalized coordinate q_1 describing the system. It is straightforward to choose the angle φ , which gives the Cartesian coordinates as

$$\begin{pmatrix} x \\ y \end{pmatrix} = \begin{pmatrix} l \cos(\varphi) \\ l \sin(\varphi) \end{pmatrix} \quad (2.3)$$

and automatically satisfies (2.2).

The Lagrange equations of the second kind are given as

$$\frac{d}{dt} \left(\frac{\partial L}{\partial \dot{q}_j} \right) - \frac{\partial L}{\partial q_j} = 0 \quad j = 1, \dots, f, \quad (2.4)$$

with the Lagrangian [14]

$$L = T - V, \quad (2.5)$$

where $T(\dot{q})$ contains the kinetic energy and $V(q)$ the potential energy of the system and the Lagrangian is a function of the coordinates q , the corresponding generalized velocities \dot{q} and time t . Here we used:

$$q = \{q_1, \dots, q_f\} \quad \dot{q} = \{\dot{q}_1, \dots, \dot{q}_f\} \quad (2.6)$$

Contrary to the $3N$ differential equations and R algebraic equations for the Lagrange equations of the first kind, we have only $3N - R$ differential equations.

2.2.2 Hamilton formalism

The Hamilton formalism provides a different formulation of classical mechanics, that can be used in many areas in physics, most prominently maybe, in its extension to quantum mechanics [14]. To calculate the Hamiltonian H of a system, the first step is the calculation of the canonical momenta

$$p_j = \frac{\partial L(q, \dot{q}, t)}{\partial \dot{q}_j}, \quad (2.7)$$

which indirectly have already been used in (2.4). In general the potential V has no dependencies on the velocities \dot{q} and the canonical momenta are

$$p_j = \frac{\partial T(q, \dot{q}, t)}{\partial \dot{q}_j}. \quad (2.8)$$

Now the generalized velocities can be written as a function of the canonical momenta, the generalized coordinates and time $\dot{q}_j = \dot{q}_j(q, p, t)$ and have to be eliminated in the Lagrangian, which then is a function of q , p and t , $L(q, p, t)$. With that, the Hamiltonian is given as [12]:

$$H(q, p, t) = \sum_{j=1}^f \dot{q}_j(q, p, t)p_j - L(q, p, t) \quad (2.9)$$

If, as in most cases, the first term in (2.9) equals $2T$, H is the energy of the system. This correspondence is a very important feature of the Hamilton formalism, especially with its application in quantum mechanics. Using (2.4), the so called canonical equations can be derived as partial derivatives of H [12]:

$$\dot{p}_j = -\frac{\partial H(q, p, t)}{\partial q_j} \quad (2.10)$$

$$\dot{q}_j = \frac{\partial H(q, p, t)}{\partial p_j} \quad (2.11)$$

2 Basics

So the equations of motion in the Hamilton formalism are $2f$ differential equations of first order for q_j and p_j , that replace the f differential equations of second order for q_j from (2.4).

2.3 Schrödinger equation

The fundamental equation in quantum mechanics is the Schrödinger equation postulated by Erwin Schrödinger in 1926. Since then, with this equation many problems could be understood and solved, like the spectrum of the hydrogen atom or the alpha decay.

The time-dependent Schrödinger equation for a free particle reads

$$i\hbar \frac{\partial}{\partial t} \psi(\mathbf{r}, t) = -\frac{\hbar^2}{2m} \nabla^2 \psi(\mathbf{r}, t) = H\psi(\mathbf{r}, t), \quad (2.12)$$

where H denotes the Hamiltonian operator of the system. This is an equation for the plane wave function $\psi(\mathbf{r}, t)$, that describes the system. As in Section 2.2 already discussed, the H operator originates from the Hamiltonian theory of mechanics and corresponds to the total energy of the system. H is the sum of a kinetic and a potential part, and for a particle moving in a potential $V(\mathbf{r}, t)$ with the energy

$$E = \frac{\mathbf{p}^2}{2m} + V(\mathbf{r}, t), \quad (2.13)$$

the Hamilton operator of the system is given as

$$H = -\frac{\hbar^2}{2m} \nabla^2 + V(\mathbf{r}, t). \quad (2.14)$$

Now the Schrödinger equation for a particle in a potential reads [15]:

$$i\hbar \frac{\partial}{\partial t} \psi(\mathbf{r}, t) = -\frac{\hbar^2}{2m} \nabla^2 \psi(\mathbf{r}, t) + V(\mathbf{r}, t) \psi(\mathbf{r}, t) \quad (2.15)$$

For (2.14) the correspondences for the energy and the momenta [16]

$$E \rightarrow i\hbar \frac{\partial}{\partial t} \quad \text{and} \quad \mathbf{p} \rightarrow \frac{\hbar}{i} \nabla \quad (2.16)$$

2 Basics

have been used.

For a Hamilton operator H independent of time, the time dependency of the Schrödinger equation can be separated with the ansatz [15]:

$$\psi(\mathbf{r}, t) = \varphi(\mathbf{r})e^{-iEt/\hbar} \quad (2.17)$$

With that the time-independent Schrödinger equation reads

$$H\varphi(\mathbf{r}) = E\varphi(\mathbf{r}), \quad (2.18)$$

which has the form of an eigenvalue equation for the Hamilton operator H .

2.4 Franck-Condon principle

An electronic transition in a molecule results in a different potential energy surface for the nuclei. This leads to another vibrational frequency of the nuclei, and that directly influences the absorption spectrum of the system, which can be measured. To look upon these effects, the Franck-Condon principle is introduced.

The principle follows from the Born-Oppenheimer approximation discussed in Section 3 and relies on the high mass ratio of nuclei and electrons to state, that the nuclei stay in position R_e during the actual electronic transition and reposition immediately afterward to R'_e . In Figure 2.1 the classical and the corresponding quantum mechanical illustration are shown. In both plots two

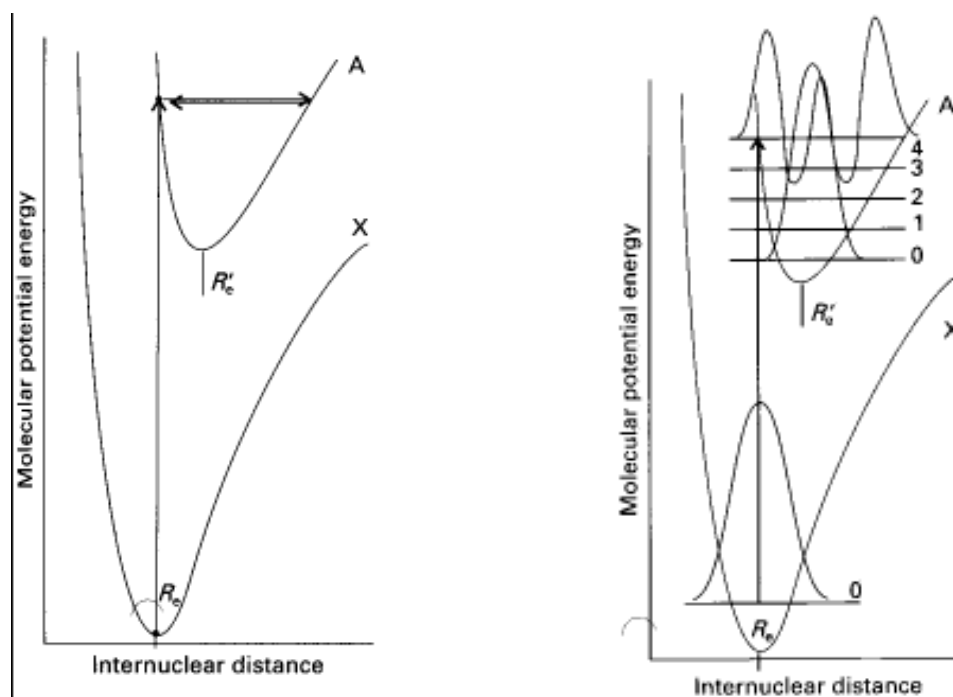


Figure 2.1: The classical and the quantum mechanical graphical illustration of the Franck-Condon principle. Both pictures are taken from [17, pp. 380].

2 Basics

potentials for a molecule are plotted with the equilibrium bond lengths R_e and R'_e , respectively. The Franck-Condon principle says, that, as an electron gets excited, the nuclei change from the ground state vibrational mode ψ_v of the R_e curve to the vibrational mode $\psi_{v'}$ of the R'_e curve with the largest overlap to the original mode.

Within the Franck-Condon principle, the electric dipole transition moment $\mu = \mu_e + \mu_N$ from the ground state $|\epsilon v\rangle$ to the excited state $|\epsilon' v'\rangle$ can be calculated as [17]:

$$\begin{aligned}
 \langle \epsilon' v' | \mu | \epsilon v \rangle &= \int \psi_{\epsilon'}^*(\mathbf{r}; \mathbf{R}) \psi_{v'}^*(\mathbf{R}) (\mu_e + \mu_N) \psi_{\epsilon}(\mathbf{r}; \mathbf{R}) \psi_v(\mathbf{R}) d\tau_e d\tau_N = \\
 &= \langle v' | v \rangle \int \psi_{\epsilon'}^*(\mathbf{r}; \mathbf{R}) \mu_e \psi_{\epsilon}(\mathbf{r}; \mathbf{R}) d\tau_e + \\
 &\quad + \langle \epsilon' | \epsilon \rangle \int \psi_{v'}^*(\mathbf{R}) \mu_N \psi_v(\mathbf{R}) d\tau_N \\
 &= \mu_{\epsilon' \epsilon} \langle v' | v \rangle
 \end{aligned} \tag{2.19}$$

In the last step it has been used, that the electron wave functions are orthogonal to each other, so the scalar product vanishes. The nuclear coordinates $\{\mathbf{R}\}$ are only parameters for the electron wave functions, which is a result of the Born-Oppenheimer approximation, and allows to assume, that the scalar product of the electron wave functions is independent of the nuclei positions.

The square of the overlap integral is called the Franck-Condon factor $\text{FC}(v', v)$ [11]:

$$\text{FC}(v', v) = |\langle v' | v \rangle|^2 \tag{2.20}$$

3 Theory

In this work we calculate the optical properties of small silver clusters from first principles. To accomplish this, the first task is to find the solution of the Schrödinger equation for a system of silver atoms. From that the electronic structure of the system and further properties can be determined. For solving the Schrödinger equation of a molecule, different methods are available. One of the first established methods is the Hartree-Fock method. Here the total wave function of the system is approximated by a Slater determinant of the one electron orbitals. The electrons move in an effective potential and do not directly interact with each other. The Schrödinger equation is now evaluated for these one electron wave functions in the effective potential.

Density functional theory (DFT) follows a different approach: Contrary to the one electron wave functions in the Hartree-Fock method, the electron density of the system plays the central role. The electron density $n(\mathbf{r})$ describes the probability to find dN electrons in the volume element d^3r at position \mathbf{r} . Owing to a theorem by Hohenberg and Kohn [18], all other features of the system are computable as functionals from the electron density. The major advantage over Hartree-Fock method is that for an N electron system the electron density is not dependent on $3N$ spatial coordinates of one electron wave functions, but only on the 3 spatial coordinates!

Both methods make use of the Born-Oppenheimer approximation. Within this approximation the motion of the nuclei is separable from the motion of the electrons. It assumes, that the electrons with the small mass compared to the nuclei, can instantly follow the slow movements of the nuclei. This is a huge simplification to the problem for fixed nuclear positions.

Using DFT the total energy of a system can be computed and furthermore the geometry of the ground state can be determined. This is the state where the energy is minimal. Varying $\{\mathbf{R}\}$ and computing the corresponding energy $E(\{\mathbf{R}\})$ of the system gives the energy as a function of the coordinates $\{\mathbf{R}\}$.

3 Theory

This is called a potential energy surface (PES). From that, the optimal geometrical arrangement of the nuclei can be found by searching for the absolute minimum of the energy.

While the determination of the equilibrium geometry only requires knowledge about the electronic ground state of a system, the calculation of optical properties asks for electronically excited states. These can be calculated with different methods. In this thesis, time-dependent density functional theory (TDDFT) will be used. This is an extension of DFT and uses a time-dependent electron density for its calculation.

In connection with the vibronic energy levels of the system the spectrum can be improved and better predictions are possible.

3.1 Density Functional Theory

As has already been mentioned before, finding the energy of a cluster of atoms or a molecule, and therefore solving the corresponding Schrödinger equation of the system, is a major problem in quantum mechanics. There are different methods available, but in this thesis we will concentrate on density functional theory (DFT). This chapter shall give a basic understanding to this topic. Further information can be found elsewhere [18, 19, 20].

The full Schrödinger equation depends on all coordinates of the nuclei and the electrons. Within the Born-Oppenheimer approximation, the movements of the electrons and the much heavier nuclei are separated. This is justified by the assumption, that the electrons can follow the nuclei adiabatically. The Schrödinger equation can then be solved in its time-independent form for fixed positions of the nuclei.

In the next step, the many-electron Schrödinger equations ought to be solved for the electrons of the system. Silver has the atomic number $Z = 47$. In this work we look at small silver clusters, for example in Ag_3 there are $N = 3 \cdot Z = 141$ electrons. Thus the Schrödinger equation has to be solved for $3 \cdot N = 423$ coordinates.

The solution of this many-electron Schrödinger equation poses severe difficulties since the complexity of the problem scales exponentially with the number of electrons. At this point the electron density $n(\mathbf{r})$ provides an alternative. The electron density of the system is dependent on just three spatial coordinates and it is incorporated in the formalism of density functional theory. The foundation of DFT are two theorems found by Hohenberg and Kohn in 1964. The first theorem says [21]:

The external potential $v(\mathbf{r})$ is determined, to within an additive constant, by the electron density $n(\mathbf{r})$.

This tells us that one can derive the external potential of the system from the electron density of a system. Furthermore, all properties of an N electron system can be determined via the electron density of the system. These

3 *Theory*

quantities are defined as functionals of the electron density. A functional is not to be confused with a function. While a function maps one number onto another, a functional maps a whole function onto one number. For example the total energy of the system is defined as a functional of the electron density function:

$$E[n(\mathbf{r})] = F[n(\mathbf{r})] + \int v(\mathbf{r})n(\mathbf{r})dr \quad (3.1)$$

where $F[n(\mathbf{r})]$ is the universal functional containing the kinetic energy and the interactions of the electrons. This equation can be found in [18].

The second theorem states that:

For a trial density $\tilde{n}(\mathbf{r})$, such that $\tilde{n}(\mathbf{r}) \geq 0$ and $\int \tilde{n}(\mathbf{r}) dr = N$,

$$E_0 \leq E[\tilde{n}(\mathbf{r})], \quad (3.2)$$

where $E[\tilde{n}(\mathbf{r})]$ is the energy functional given in (3.1), and E_0 is the ground state of the system. [21].

What follows from this theorem is that the electron density minimizing the energy functional in (3.1) is the exact electron density of the ground state.

These two theorems can be used to derive a procedure to find the electron density of the system in question. This instruction has been found by Kohn and Sham in 1965 [18] and the set of equations is called after them the Kohn-Sham equations. The universal functional for the Kohn-Sham equations contains another term called the exchange-correlation energy $E_{XC}[n(\mathbf{r})]$ containing quantum mechanical exchange of electrons and electron correlation:

$$F[n(\mathbf{r})] = T_0[n(\mathbf{r})] + U[n(\mathbf{r})] + E_{xc}[n(\mathbf{r})] \quad (3.3)$$

Their scheme makes it possible to calculate the electron density iteratively and moreover quite simply. That is because every equation has to be solved for just a single electron.

For the description of the Kohn-Sham equations Kohn's Nobel lecture has been

3 Theory

used, see [18]. The formalism starts with a trial electron density $n_1(\mathbf{r})$ and N equations for the not interacting electrons φ_i :

$$\left(-\frac{1}{2}\nabla^2 + v_{\text{eff}}(\mathbf{r})\right)\varphi_i(\mathbf{r}) = \epsilon_i\varphi_i(\mathbf{r}) \quad (3.4)$$

The effective potential that contains all the interaction of the electrons is given by

$$v_{\text{eff}}(\mathbf{r}) = v_{\text{ext}}(\mathbf{r}) + v_H(\mathbf{r}) + v_{\text{xc}}(\mathbf{r}). \quad (3.5)$$

The external potential, the Hartree potential and the exchange-correlation potential are given by

$$v_{\text{ext}}(\mathbf{r}) = -\sum_i \frac{Z_i}{|\mathbf{r} - \mathbf{R}_i|} \quad (3.6)$$

$$v_H(\mathbf{r}) = \int \frac{n(\mathbf{r}')}{|\mathbf{r} - \mathbf{r}'|} d\mathbf{r}' \quad (3.7)$$

$$v_{\text{xc}}(\mathbf{r}) = \frac{\delta E_{\text{xc}}[n(\mathbf{r})]}{\delta n(\mathbf{r})} \quad (3.8)$$

The quantity $v_{\text{ext}}(\mathbf{r})$ describes the Coulomb interaction of the electrons with the nuclei, $v_H(\mathbf{r})$ contains the Hartree interaction of the electrons. The exchange-correlation potential is defined as a functional derivative of the exchange-correlation energy $E_{\text{xc}}[n(\mathbf{r})]$ with respect to the electron density. The exchange-correlation energy is defined to contain all interactions not considered in the other terms. The one electron equations (3.4) can now be solved for the N eigenfunctions $\varphi_i(\mathbf{r})$. These eigenfunctions yield the electron density of the system:

$$n(\mathbf{r}) = \sum_{i=1}^N |\varphi_i(\mathbf{r})|^2 \quad (3.9)$$

The Kohn-Sham equations (3.4) together with the definition of the effective potential (3.6)-(3.8) and the electron density (3.9) have to be solved self-consistently [20]. After each iteration a new trial density has to be computed from the just calculated density from equation (3.9) and the density from previous iterations. A convergence criterion defined at the beginning of the calculation is applied at this point on the electron density that determines the

3 Theory

final density is reached.

There are different ways to calculate the new trial electron density $n_{i+1}(\mathbf{r})$. A simple way would be

$$n_{i+1} = \alpha n_i + (1 - \alpha) n_{i-1} \quad (3.10)$$

with the mixing parameter α .

The crucial part of the Kohn-Sham equations is the exchange-correlation energy $E_{xc}[n]$. Its exact form is only known for the uniform electron gas [19]. For non-uniform electron densities, suitable approximations have to be found. First, the simplest approximation of $E_{xc}[n]$ is the local density approximation (LDA) [22]:

$$E_{xc}^{\text{LDA}}[n] = \int e_{xc}^{\text{uniform}}(n(\mathbf{r}))n(\mathbf{r})d\mathbf{r} \quad (3.11)$$

Here $e_{xc}^{\text{uniform}}(n)$ denotes the exchange-correlation energy per particle of the uniform electron gas of the density n [18]. It may seem as a crude approximation to use $e_{xc}^{\text{uniform}}(n)$ for the density of the uniform electron gas is constant at all positions in space. Interestingly enough LDA has proven to work surprisingly well even for systems which are far from uniform electron gas. Many properties can be described with satisfactory accuracy with this, compared to other methods, simple approximation [22]. The local spin density approximation (LSDA) is an extension of LDA including spin. The next step in approximating the exchange-correlation energy is to add a dependency of the gradient of the electron density at \mathbf{r} , which leads to the so-called generalized gradient approximation (GGA) [23]:

$$E_{xc}^{\text{GGA}}[n_{\uparrow}, n_{\downarrow}] = \int f_{xc}(n_{\uparrow}, n_{\downarrow}, \vec{\nabla}n_{\uparrow}, \vec{\nabla}n_{\downarrow})n(\mathbf{r})d\mathbf{r} \quad (3.12)$$

Once the energy of the ground state of a system is computed, it can be used for structure optimizations. Also, ground state DFT calculations present the starting point of TDDFT, the calculation of excited states. This is the topic of the next chapter.

3.2 Time dependent Density Functional Theory

Density functional theory has proven to be very useful for the description of ground state properties of a system. For many applications, however the calculation of the excited states of a system is essential. From the development of the Kohn-Sham equations to the extension of a time dependent treatment some years have passed. In 1984 Runge and Gross proved a theorem stating that the time dependent density uniquely determines the time dependent external potential and vice versa:

For every single-particle potential $v(\mathbf{r}, t)$ which can be expanded into a Taylor series with respect to the time coordinate around $t = t_0$, a map $G : v(\mathbf{r}, t) \rightarrow n(\mathbf{r}, t)$ is defined by solving the time-dependent Schrödinger equation with a fixed initial state $\Phi(t_0) = \Phi_0$ and calculating the corresponding densities $n(\mathbf{r}, t)$. This map can be inverted up to an additive merely time-dependent function in the potential [24, p. 998].

This theorem can be seen as the analogon of the Hohenberg-Kohn theorems for the time-independent case. So again, if the exact time-dependent electron density of a system is known, all other properties of the system can be calculated. The digression from $3N$ spatial coordinates to 3 coordinates is the same as for the time-independent case.

The role of minimizing the total energy in the time-independent case is taken here by the variation of the action A of the system:

$$A = \int_{t_0}^{t_1} \left\langle \Psi(t) \left| i \frac{\partial}{\partial t} - \hat{H}(t) \right| \Psi(t) \right\rangle dt \quad (3.13)$$

If the functional derivative of the action with respect to the density gives zero, the proper density $n(\mathbf{r}, t)$ has been found [25]:

$$0 = \frac{\delta A}{\delta n(\mathbf{r}, t)} = \int_{t_0}^{t_1} \left\langle \frac{\delta \Psi(t')}{\delta n(\mathbf{r}, t)} \left| i \frac{\partial}{\partial t'} - \hat{H}(t') \right| \Psi(t') \right\rangle dt' + const. \quad (3.14)$$

3 Theory

Now the Kohn-Sham equations in their time-dependent form can be formulated. The density for the non interacting electrons φ_i is given as

$$n(\mathbf{r}, t) = \sum_i^{occ} \varphi_i^*(\mathbf{r}, t) \cdot \varphi_i(\mathbf{r}, t). \quad (3.15)$$

The time-dependent Schrödinger equation for non interacting electrons looks quite similar to (3.4) except for the time dependency [26]:

$$\left(-\frac{1}{2}\nabla^2 + v_{\text{eff}}(\mathbf{r}, t)\right) \varphi_i(\mathbf{r}, t) = i \frac{\partial}{\partial t} \varphi_i(\mathbf{r}, t) \quad (3.16)$$

The effective potential v_{eff} is given by

$$v_{\text{eff}}(\mathbf{r}, t) = v_{\text{ext}} + \underbrace{\int \frac{n(\mathbf{r}', t)}{|\mathbf{r} - \mathbf{r}'|} d\mathbf{r}'}_{v_{\text{SCF}}(\mathbf{r}, t)} + v_{\text{xc}}(\mathbf{r}, t). \quad (3.17)$$

Here, v_{ext} denotes the attraction of the nuclei and v_{SCF} is the self consistent field potential. The role of the energy is now taken by the action of the system and therefore the time-dependent exchange-correlation potential can be written as the derivative of the action with respect to the density [27]:

$$v_{\text{xc}}(\mathbf{r}, t) = \frac{\delta A_{\text{xc}}[n(\mathbf{r}, t)]}{\delta n(\mathbf{r}, t)} \quad (3.18)$$

3.2.1 Casida formalism

For a small perturbation of the system a linear response approach can be used. One way to formulate linear response is the so-called Casida formalism which is also utilized in the ABINIT code which has been used for the calculations of this thesis. As ABINIT uses the Casida formalism this approach will be described shortly. The perturbation v_{pert} is added to the effective potential in the Kohn-Sham equations:

$$v_{\text{eff}}(\mathbf{r}, t) = v_{\text{ext}} + v_{\text{SCF}}(\mathbf{r}, t) + v_{\text{pert}}(\mathbf{r}, t). \quad (3.19)$$

3 Theory

The change of v_{eff} due to the introduction of v_{pert} is given by

$$\delta v_{\text{eff}}(\mathbf{r}, t) = \delta v_{\text{SCF}}(\mathbf{r}, t) + \delta v_{\text{pert}}(\mathbf{r}, t). \quad (3.20)$$

The linear response of the density matrix arising from the change in the potential can be expressed in second quantization notation as

$$\delta P_{ij\sigma}(\omega) = \frac{f_{j\sigma} - f_{i\sigma}}{\omega - (\epsilon_{i\sigma} - \epsilon_{j\sigma})} \delta v_{ij\sigma}^{\text{eff}}(\omega). \quad (3.21)$$

In this notation the Greek index corresponds to spin while the Latin letters refer to space coordinates. The basis are the unperturbed molecular orbitals where the $f_{i\sigma}$ denote the occupation numbers and the $\epsilon_{i\sigma}$ the eigenenergies of the orbitals [25]. The connection of v_{SCF} to the density matrix is given with the use of the coupling matrix \hat{K} in the following way:

$$\delta v_{ij\sigma}^{\text{SCF}}(\omega) = \sum_{kl\tau} K_{ij\sigma,kl\tau}(\omega) \delta P_{kl\tau} \quad (3.22)$$

And the coupling matrix is given by [28]:

$$K_{ij\sigma,kl\tau} = \int \int \varphi_{i\sigma}^*(\mathbf{r}) \varphi_{j\sigma}(\mathbf{r}) \left(\frac{1}{|\mathbf{r} - \mathbf{r}'|} + \frac{\partial v_{\sigma}^{\text{xc}}(\mathbf{r})}{\partial n_{\tau}(\mathbf{r}')} \right) \varphi_{k\tau}(\mathbf{r}') \varphi_{l\tau}^*(\mathbf{r}') d\mathbf{r} d\mathbf{r}' \quad (3.23)$$

Further calculation allows one to define the matrix $\hat{\Omega}$ [25]:

$$\begin{aligned} \Omega_{ij\sigma,kl\tau}(\omega) = & \delta_{\sigma,\tau} \delta_{i,k} \delta_{j,l} (\epsilon_{l\tau} - \epsilon_{k\tau})^2 \\ & + 2\sqrt{(f_{i\sigma} - f_{j\sigma})(\epsilon_{j\sigma} - \epsilon_{i\sigma})} K_{ij\sigma,kl\tau}(\omega) \sqrt{(f_{k\tau} - f_{l\tau})(\epsilon_{l\tau} - \epsilon_{k\tau})}, \end{aligned} \quad (3.24)$$

whose eigenvalues are the squares of the excitation energies ω_n :

$$\hat{\Omega}(\omega) \mathbf{F}_n = \omega_n^2 \mathbf{F}_n \quad (3.25)$$

Also the oscillator strengths f_n can be calculated from this equation using the eigenvectors \mathbf{F}_n . With the oscillator strengths and the excitation energies at

3 Theory

hand, the calculation of the spectrum is easy with the dynamic polarizability α [26]:

$$\alpha(\omega) = \sum_n \frac{f_n}{\omega_n^2 - \omega^2} \quad (3.26)$$

4 Results

The theoretical tools described in the previous Chapter 3 form the basis for the problems proposed in Chapter 1. For the implementation of density functional theory the open source program package ABINIT has been used. Further information on how ABINIT works can be found in [29].

First convergence parameters had to be tested to find appropriate values for each one. Next these parameters were used to find the equilibrium structures of the different clusters. At this step an interesting feature has been found for Ag_3 : The calculations suggest two structures for the equilibrium, a nearly linear formation of the atoms and a equilateral triangular formation. In literature on the structure of Ag_3 , for example [2, 3, 7, 6, 4], the almost linear structure has not been discussed. Therefore a special attention has been laid on the two possible structures of Ag_3 .

With the equilibrium configuration found, the next step were the TDDFT calculations. From the excitation energies and the oscillator strengths the spectra were built and compared to spectra derived from experiments. The exchange-correlation functionals are for LDA the Perdew-Wang 92 functional [30], which has been used for both ground state and excited states calculation, and for GGA the Perdew-Burke-Enzerhof functional [23] for ground state calculations.

The calculations for the vibronic spectra were computed with the program *Mathematica*.

4.1 Convergence Parameters

The results of ab-initio (TD)DFT calculations do not depend on adjustable parameters. However, there are a number of so-called convergence parameters which, for example, define the size of the basis set or the size of the simulation cell, which have to be determined. In order to determine suitable values for these convergence parameters, a quantity of interest, such as the total energy or the equilibrium geometry, is calculated as a function of the convergence parameter. From this dependence, together with a targeted precision, the value of the convergence parameter can be obtained. Thereby parameters, which lead to a minimum of computational effort at a target accuracy, are determined.

To find the appropriate parameters, the calculations of the total energy for Ag_2 were done for different values of the parameters while changing the bond length between the atoms. By plotting the total energy for different values of the bond length we get a curve with a minimum of the energy at the equilibrium bond length of the dimer. To extract the ground state distance we fit the data with a cubic polynomial and extract the minimum. This has to be done for different values of the parameters. In a diagram where the equilibrium bond length versus the parameter values is plotted, we can see for example in the figures 4.3, 4.4, or 4.5, that for better values of the parameters, the bond length reaches convergence. The same can be done to the parameter ω for the quadratic term in the fit. Now the task is to find the value that gives rise to a low computation cost at one hand and on the other hand provides acceptable results.

Such plots have been generated for the parameters *ecut*, *acell* and *nband*. *ecut* is used in the Kohn-Sham equations and determines the kinetic energy cut-off and therefore the number of plane waves to represent the wave function. The parameter *acell* sets the size of the cell in which the molecule is located. Because ABINIT works with periodic boundary conditions, the values of this parameter should be chosen big enough such that there is no interaction between the periodic replica of molecules. In Figure 4.1 one sees the concept of periodic boundary conditions in two dimensions. The cell in the middle has

4 Results

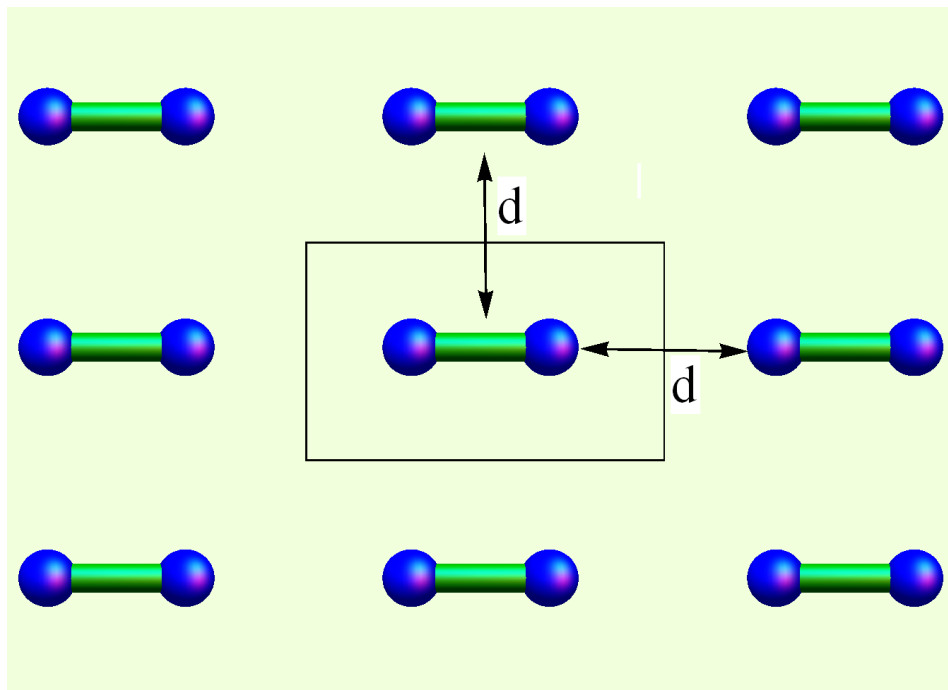


Figure 4.1: The concept of periodic boundary conditions in 2D. d labels the inter-cell distance used as convergence parameter.

eight neighbor molecules and the convergence parameter used is the inter-cell distance d , which is the minimum distance to the next neighbor molecule. Note, that the actual calculations use periodic boundary conditions in three dimensions. The third parameter $nband$ determines the number of electronic states used in the calculation. The number of unoccupied states is a convergence parameter for TDDFT calculations. See Section 3.1 for further details on these parameters. For all three parameters, the computation time increases as the value of the parameter increases. We can see this in Figure 4.2, where for different values of $nband$ and $ecut$ the CPU time for the TDDFT-calculation of N_2 is plotted. Additionally this figure tells us that the CPU time is more sensitive to a larger number of bands in the calculation than an increase of the value of $ecut$.

The following figures show the convergence for the three parameters $ecut$, $nband$ and $acell$. For ground state calculations, the number of bands has to be just

4 Results

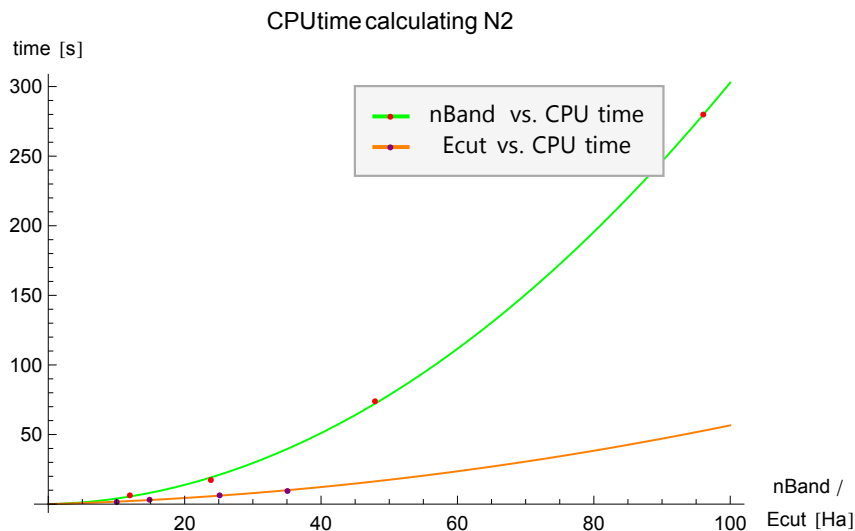


Figure 4.2: The CPU time for the DFT-calculation of N_2 for different values of $ecut$ and $nband$.

larger than the number of valence electrons. This is because the unoccupied bands do not play a role in the ground state calculation. So the number of bands for DFT calculations is set to 20 for Ag_2 . In Figure 4.3 the ground state distance d is plotted for different values of $ecut$. The plot contains the minimum distances d for the ground state as well as for the first excited state which are referred to as $E0$ and $E1$, respectively. We see that for $ecut = 20Ha$ and larger values the minimum distance d does not change significantly. This applies to the ground state as well as to the first excited state.

For $nband$ the plot has only been generated for the excited states (TDDFT), because, as mentioned before, for the ground state of the system (DFT) the number of unoccupied bands has no effect on the calculation. The plot can be seen in Figure 4.4. Here convergence is reached at about 80 bands for Ag_2 giving 40 bands per atom.

The Figure 4.5 shows the convergence of the equilibrium bond length with respect to the parameter $acell$. The equilibrium bond length is sufficiently converged for a inter-cell distance $d = 22a_0$ to the next Ag_2 molecule.

To summarize the convergence of all three parameters, the deviation to the

4 Results

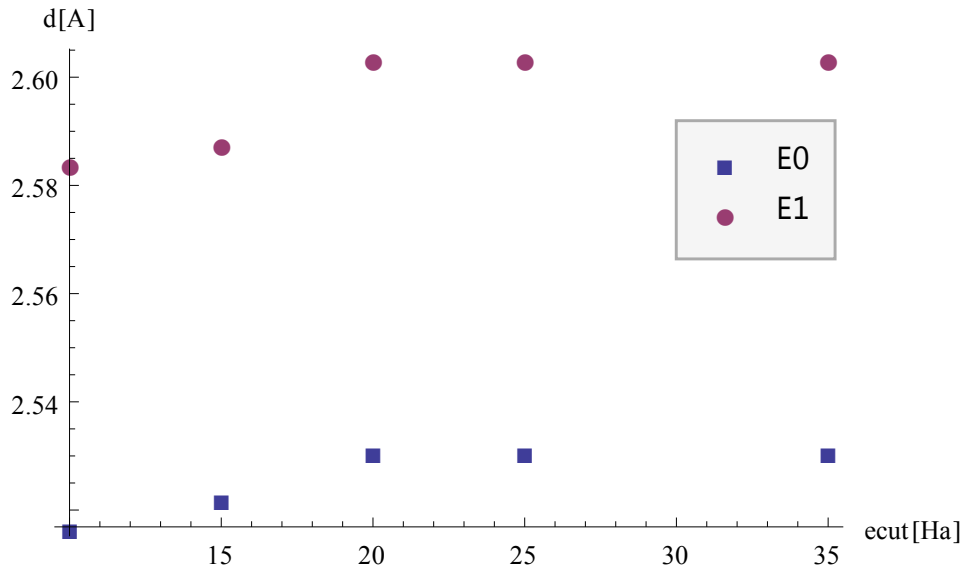


Figure 4.3: Convergence for the parameter *ecut*. For the DFT calculation of the Ag_2 system *nband* has the value 20 and for the TDDFT calculation 50 bands were used. The inter-cell distance d is $22a_0$

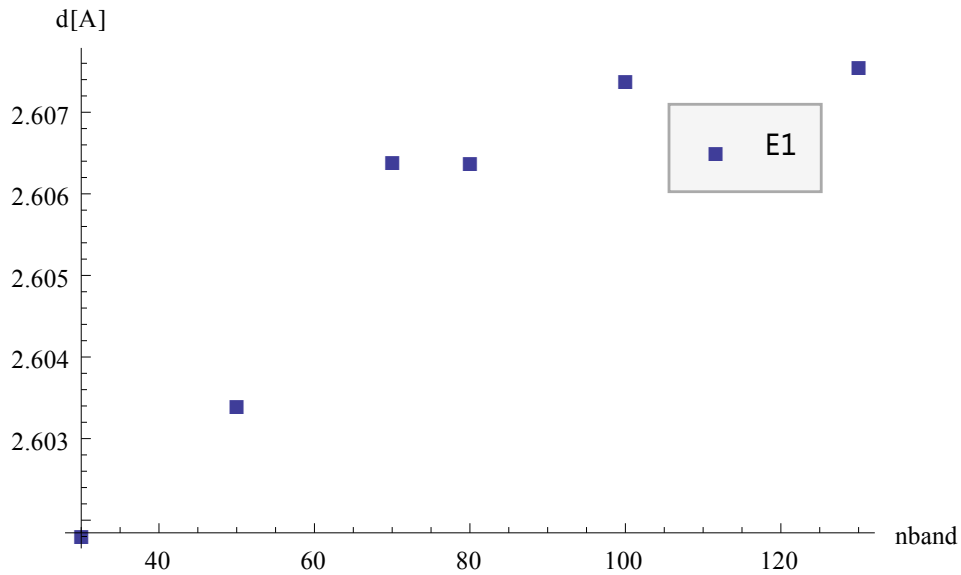


Figure 4.4: Convergence for the parameter *nband*. For the TDDFT calculation of the Ag_2 system *ecut* has the value $25Ha$, the inter-cell distance d is $22a_0$.

4 Results

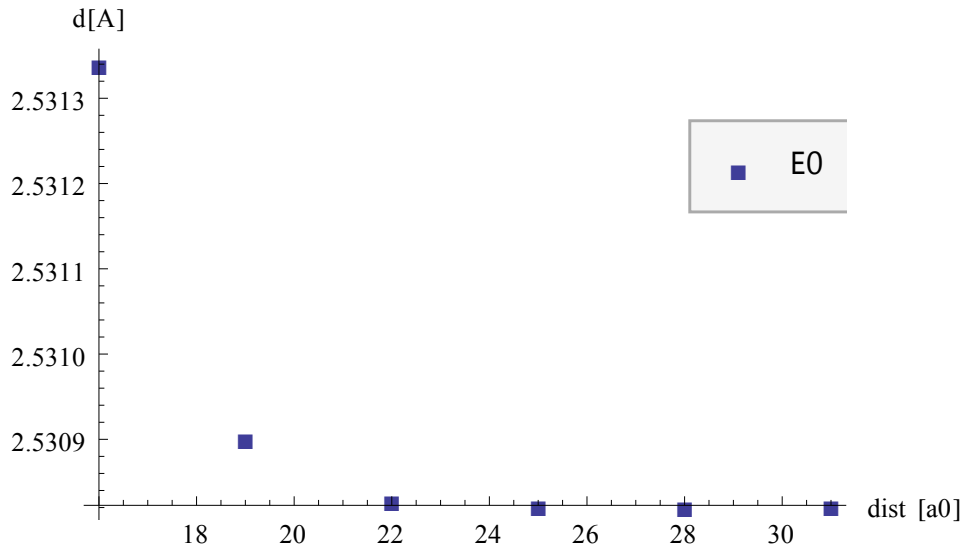


Figure 4.5: Convergence for the parameter $acell$ (inter-cell distance d). For the DFT calculation of the Ag_2 system $ecut$ has the value $25Ha$ and the number of bands $nband$ is 20.

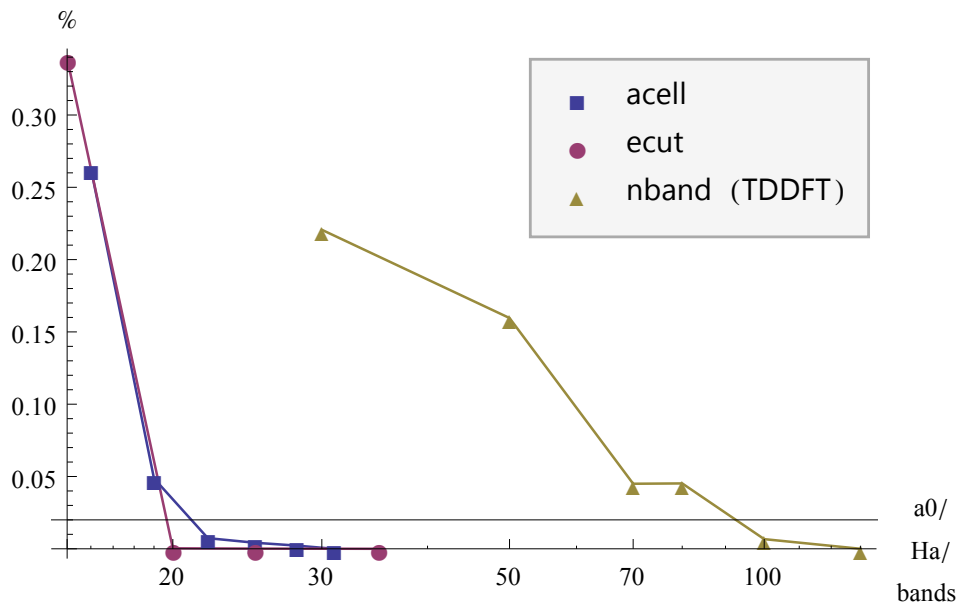


Figure 4.6: Convergence for parameters $acell$, $ecut$ and $nband$ for Ag_2 . The data has been taken from the previous plots in Figures 4.3-4.5

4 Results

converged value of all the calculations is shown in Figure 4.6. A summary of the three parameters is also given in Table 4.1.

Table 4.1: Converged parameters for DFT and TDDFT calculations derived from the Ag_2 system.

	<i>acell</i> (<i>d</i>) [a_0]	<i>ecut</i> [Ha]	<i>nband</i> [per atom]
DFT	22	25	10
TDDFT	22	25	40

4.2 Structures for the clusters Ag_2 to Ag_5

For the determination of the equilibrium structure, the total energy of a cluster has been calculated for different bond lengths and angles. The energy is then plotted as a function of the bond length. At the minimum of the total energy, the equilibrium distance is found. For Ag_2 the situation is pretty easy: There is only one parameter defining the structure, the bond distance. For larger clusters, this gets rapidly more complicated, as for every additional atom an additional parameter depicts the structure and has to be optimized to find the equilibrium structure of the cluster. For this reasons the structure optimization has only been verified by comparison to [2] for Ag_2 (1 parameter) and Ag_3 (2 parameters), for the other clusters (Ag_4 and Ag_5) the structure parameters have been taken from the same source.

4.2.1 Ag_2

The plot for the energy as a function of the distance d between the two atoms with a fit is given in Figure 4.7. The minimum energy is at $d = 2.53\text{\AA}$. The calculations have been done with the parameters derived in the previous section and are listed in the Table 4.1.

4.2.2 Ag_3

The determination of the ground state geometry for Ag_3 is somewhat more complicated because we have to vary two parameters. The first approach was to expect an equilateral triangle and thus eliminating one parameter. The remaining parameter is the length of one side. But this lead to problems: the DFT calculations did not converge because of an instability related to the degeneracy of the highest occupied molecular orbital. To take care of this

4 Results

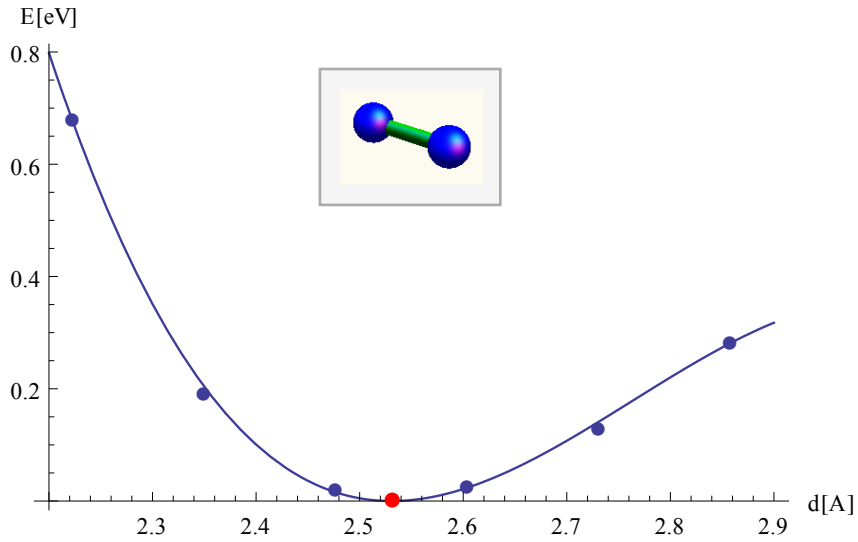


Figure 4.7: Ground state bond length calculation for Ag_2 .

problem some asymmetry has to be introduced. For example by using a second parameter and looking upon the structure of an isosceles triangle. Here the parameters used are the base length b and the length of the other two sides a , see also Figure 4.8. A plot has been generated for a calculation where for

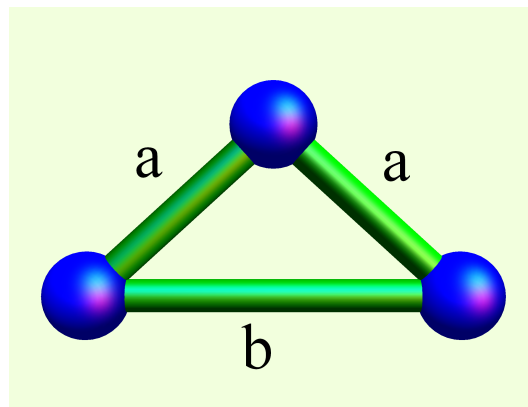


Figure 4.8: The parameters a and b used in the calculations for Ag_3 .

different values of the parameters a and b the calculated energy is plotted. This can be seen in Figure 4.9.

4 Results

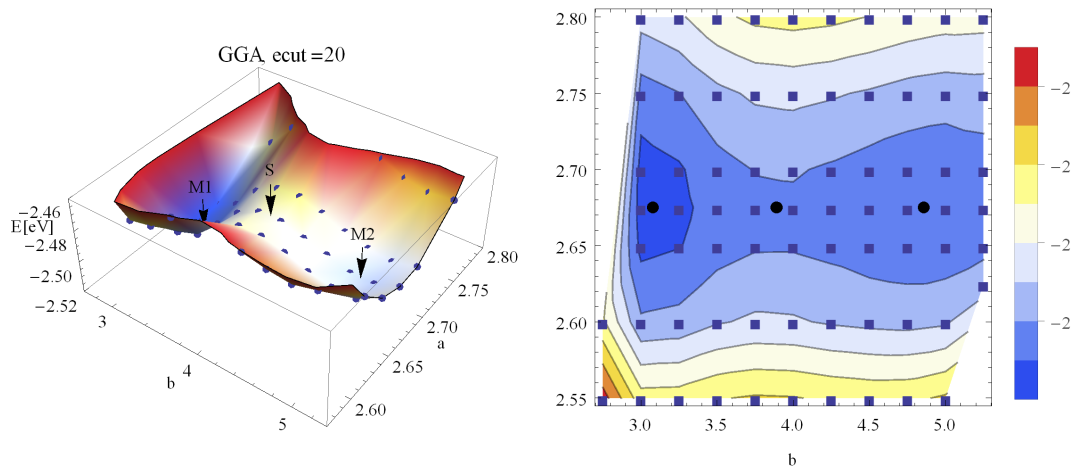


Figure 4.9: Potential energy surface of Ag_3 as a function of the two parameters a and b using GGA.

The left plot in Figure 4.9 is a plot of the potential energy surface and gives a better understanding of the form of the potential, the right plot is a density plot of the same data and shows additionally the data points used for the interpolation. At the left side of the plots the parameters form a triangle. The more one moves to the right side of the plots, the more the silver atoms are arranged in a line. The white areas in the right plot refer to points where the calculation did not converge. These points also include the cases where the parameters form an equilateral triangle.

What is surprising with these plots is, that they show two local minima. One pronounced global minimum, which corresponds to a triangular structure of the atoms, and the other minimum at a configuration, where the parameters describe a nearly linear silver trimer. These two minima and the saddle point between the minima are listed in Table 4.2. There it can be seen, that the difference of the energy between the minima and the saddle point is also very small with 30 and 14 meV, respectively. All three points have the same value for parameter a , so the minimum energy path connecting the two minima across the saddle point can be characterized by a fixed bond distance $a = 2.675\text{\AA}$.

4 Results

This energy path is shown in Figure 4.10 and contains additionally a graphic interpretation of the parameters of the silver trimer for the minima.

These calculations also have been done using LDA. Here, the minima are not

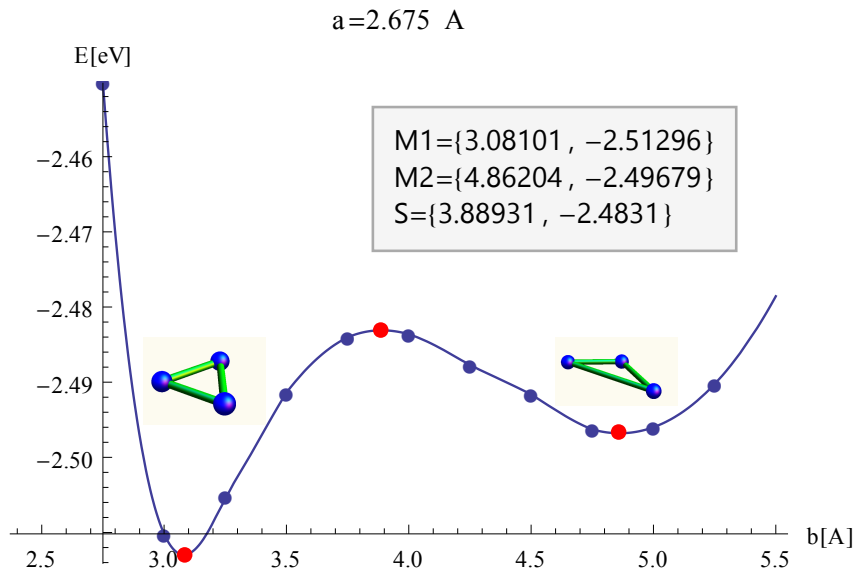


Figure 4.10: Minimum energy path connecting the two local minima using GGA. The minima and the saddle point are given as (a, b) coordinates.

that distinctive and the potential energy surface has a slightly different form, as can be seen in Figure 4.11. Additionally, it is observable, that the position of the minima has shifted to smaller bond lengths compared to GGA (see Figure 4.10). This is an effect of the well known over-binding of LDA [31, p. 5]. In Figure 4.12, the plot with the cut through the potential energy surface at the minimum of parameter a , corresponding to the plot in Figure 4.9 for GGA, is shown. The minima and the saddle point are summarized in Table 4.2. From this table one can calculate the differences of the minima to the saddle point as 125.7 meV and 0.7 meV, respectively. In comparison to the results from the GGA calculations, the first minimum is sharper in LDA, while the second minimum has nearly vanished.

4 Results

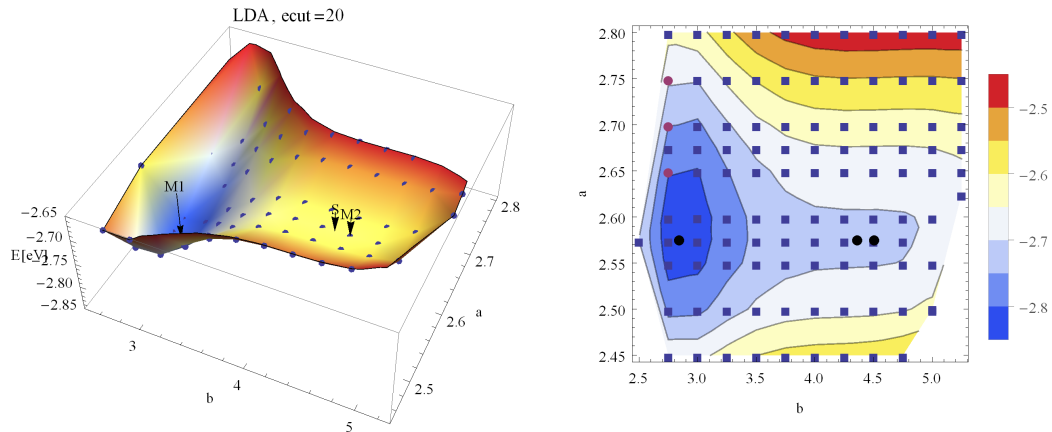


Figure 4.11: Potential energy surface of Ag_3 as a function of the two parameters a and b using LDA.

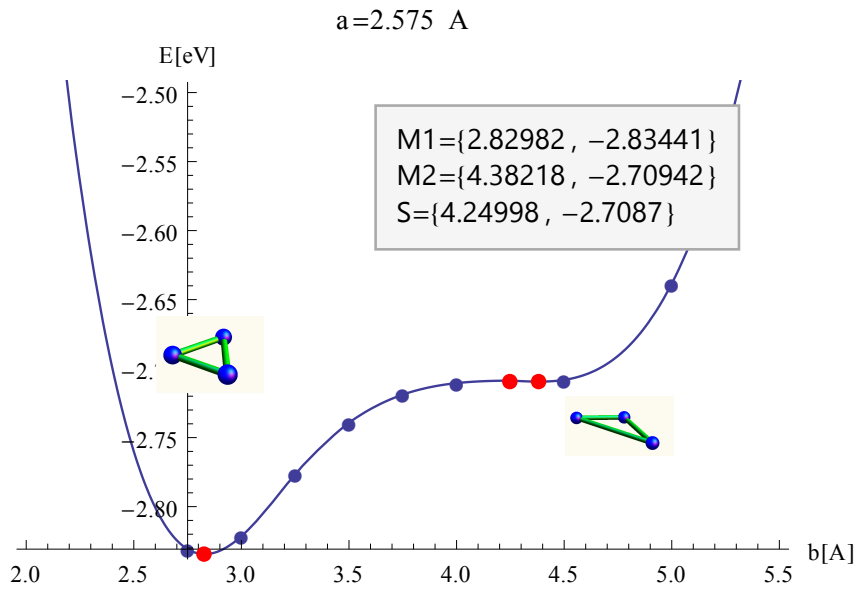


Figure 4.12: Ground state bond length calculation for Ag_3 with $a = 2.575 \text{ \AA}$ using LDA.

4 Results

Table 4.2: Minima and saddle point for Ag_3 calculated with GGA and LDA, respectively.

		a [\AA]	b [\AA]	$E - E_0$ [meV]
GGA	M_1	2.675	3.081	-2512.96
	M_2	2.675	4.862	-2496.79
	S	2.675	3.889	-2483.1
LDA	min_1	2.575	3.0627	-2834.41
	min_2	2.575	4.65236	-2709.42
	$saddle$	2.575	4.29864	-2708.7

4.2.3 Comparison

The bond length derived for Ag_2 and the structure parameters for the triangular form of Ag_3 are in good accordance to previous calculations [2, 3, 6] and experiments [10], as can be observed in Table 4.3. For the linear form of Ag_3

Table 4.3: Comparison of calculated values of Ag_2 and the triangular form of Ag_3 to values from literature calculated and experimentally found.

	d1 [\AA]	d2 [\AA]
Ag_2		
this work	2.53	
Idr. [2]	2.57	
Bon. [3]	2.52	
Fou. [6]	2.50	
expt. [10]	2.53	
Ag_3		
this work	2.675	3.081
Idr. [2]	2.64	3.068
Bon. [3]	2.58	2.88
Fou. [6]	2.67	2.986

no other reports could be found to compare the parameters with. This may be because in most works only the energetically lowest isomer is discussed. But, as in Table 4.2 or in Figure 4.10 observable, the difference of the energy between the two minima is only 16 meV. For the clusters Ag_4 and Ag_5 , the

AB INITIO CALCULATION OF SMALL SILVER CLUSTERS

4 Results

parameters calculated in [2] are taken. These parameters (bold) can be seen in Figure 4.13, which has also been taken from [2].

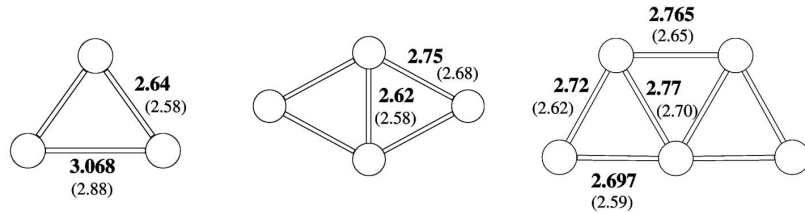


Figure 4.13: Parameters for clusters Ag_3 to Ag_5 , the bold parameters and the picture are from [2] and the parameters in brackets from [3].

4.3 Optical spectra for the clusters Ag_2 to Ag_5

To calculate the optical spectrum of a cluster, excitation energies and corresponding oscillator strengths are needed. These can be obtained, as discussed also in Section 3.2, via a TDDFT calculation: The starting point is a DFT calculation that yields the ground state Kohn-Sham orbitals $\varphi(\mathbf{r})$. These enter equation (3.23), from which the excitation energies ω_i and the oscillator strengths f_i are obtained with equations (3.24) and (3.25).

The structures given in Table 4.2 for Ag_2 and Ag_3 and in Figure 4.13 for Ag_4 and Ag_5 are used for the calculation. The spectra are compared to experimental data taken from [7], where the absorption spectra have been measured for silver clusters in an argon matrix at 7 Kelvin. The spectra are given in the form (ω_i, f_i) , which corresponds to discrete peaks. So, for a better comparison, the peaks are broadened with a Gaussian function. The absorption spectrum then has the form

$$\alpha(\omega) = \sum_n f_n e^{-\frac{(\omega - \omega_n)^2}{2\Delta^2}}, \quad (4.1)$$

with Δ being the broadening factor.

The first excitation energies with corresponding oscillator strengths larger than $f_i > 10^{-3}$ calculated for Ag are given in Table 4.4. The graphical realization of

Table 4.4: First computed excitation energies ω_i and oscillator strengths f_i with $f_i > 10^{-3}$ for Ag .

i	ω_i [eV]	f_i	main band contribution
1	3.976	$2.222 \cdot 10^{-1}$	6 \rightarrow 9, spin up
2	3.9764	$2.225 \cdot 10^{-1}$	6 \rightarrow 8, spin up
3	3.9798	$2.217 \cdot 10^{-1}$	6 \rightarrow 7, spin up
4	5.7767	$2.067 \cdot 10^{-3}$	6 \rightarrow 15, spin up
5	5.7768	$2.082 \cdot 10^{-3}$	6 \rightarrow 14, spin up
6	5.7771	$2.076 \cdot 10^{-3}$	6 \rightarrow 16, spin up

this data with Equation (4.1) is presented in Figure 4.14. As can be observed, the main peak calculated is at the same position as the one found in experiment.

4 Results

For Ag_2 the calculated excitation energies and oscillator strengths are given

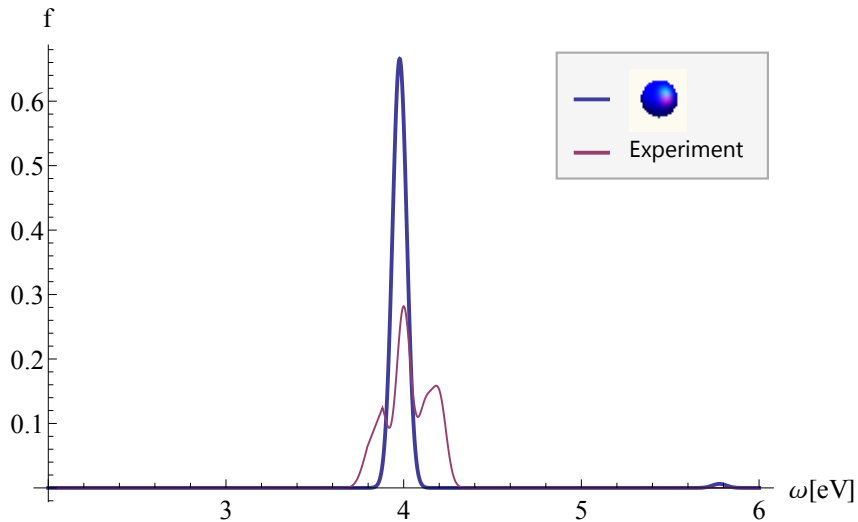


Figure 4.14: Absorption spectrum calculated for Ag_1 , the broadening factor is $\Delta = 0.04$.

in Table 4.5, the spectrum generated from this data is given in Figure 4.15. In

Table 4.5: First computed excitation energies ω_i and oscillator strengths f_i with $f_i > 10^{-3}$ for Ag_2 .

i	ω_i [eV]	f_i	main band contribution
1	3.1478	$3.234 \cdot 10^{-1}$	11 \rightarrow 12
2	3.9962	$1.044 \cdot 10^{-3}$	8 \rightarrow 12
3	3.9962	$1.044 \cdot 10^{-3}$	9 \rightarrow 12
4	4.8300	$3.528 \cdot 10^{-1}$	11 \rightarrow 14
5	4.8300	$3.528 \cdot 10^{-1}$	11 \rightarrow 13
6	5.6418	$1.710 \cdot 10^{-2}$	1 \rightarrow 12

comparison to the experimental data, a small shift of the peaks is observable. Within this shift the two spectra have peaks at nearly the same values.

The two structural forms of Ag_3 are compared to experimental data in Figure 4.16. Neither of the two structures shows a good agreement with the experimental data. What can also be seen, is that the two computed spectra differ

4 Results

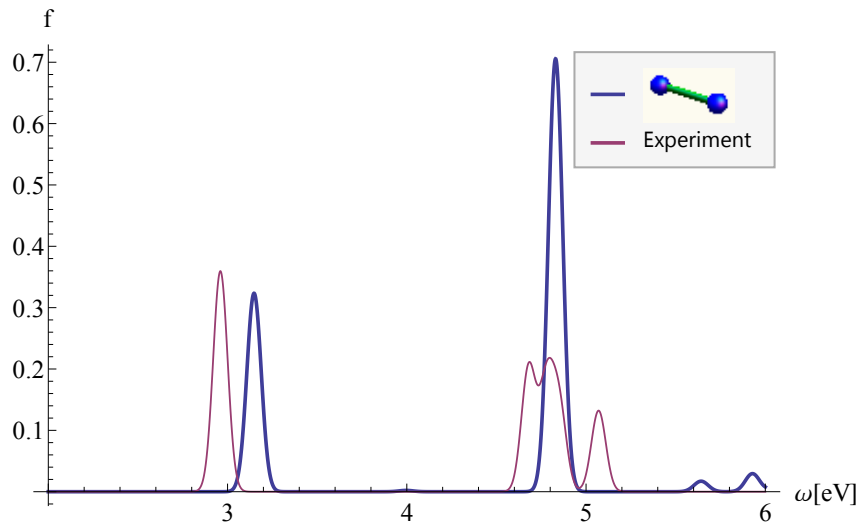


Figure 4.15: Absorption spectrum calculated for Ag_2 , the broadening factor is $\Delta = 0.04$.

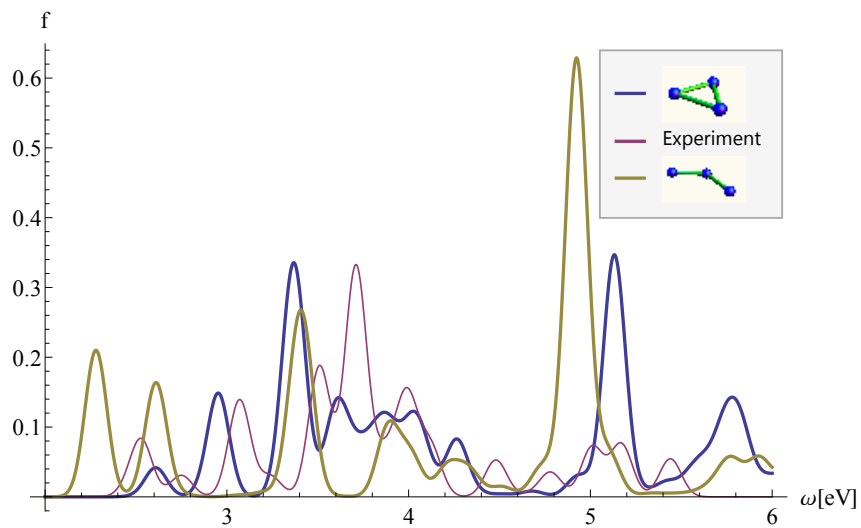


Figure 4.16: Absorption spectra calculated for Ag_3 , the broadening factor is $\Delta = 0.06$.

4 Results

also from each other profoundly. The triangular structure of Ag_3 shows excitations nearly at the same energies as the experimental data does, but the oscillator strengths do not agree at all. The two main peaks of the computed spectra at $\omega \approx 5$ eV are totally off and if ignored, a shift of some peaks due to vibronic transitions, as investigated later on, may could improve the spectra. A closer examination of the spectra for the transition from a linear structure to a triangular structure of Ag_3 has been done in Section 4.3.1.

The spectrum calculated for Ag_4 is compared to experimental data in Figure 4.17. Again, a shift of 0.14 eV is observable, i.e. the main peak in the experimental data is at 3.07 eV and at 2.93 eV in the computed spectrum. Apart from that, the oscillator strengths and the shape of the spectrum fits rather well.

In Figure 4.18 the spectrum calculated for Ag_5 is visualized and compared to

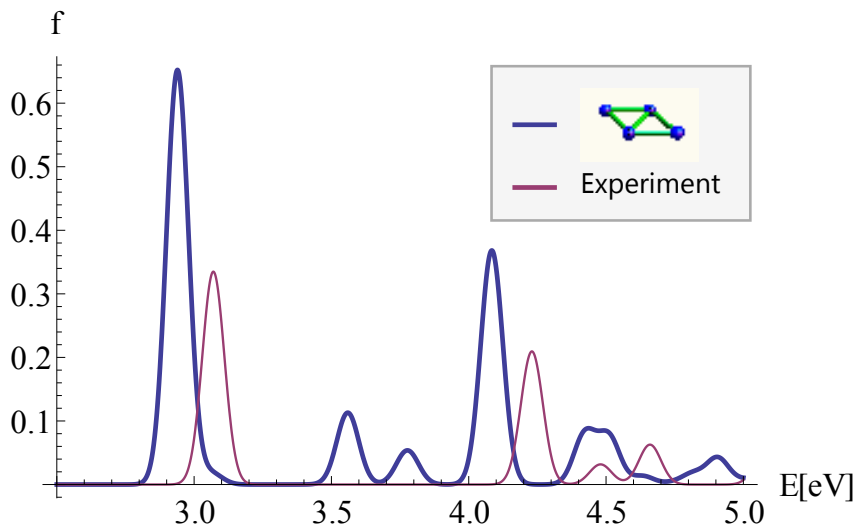


Figure 4.17: Absorption spectrum calculated for Ag_4 , the broadening factor is $\Delta = 0.04$.

experimental data. The computed spectrum shows a shift of 0.2 eV with the two main peaks at 3.18 eV and at 3.48 eV for the computed spectrum and at 3.27 eV and at 3.73 eV for the experimental data. The oscillator strengths do not match that well for this structure, but again the shape of the spectrum

4 Results

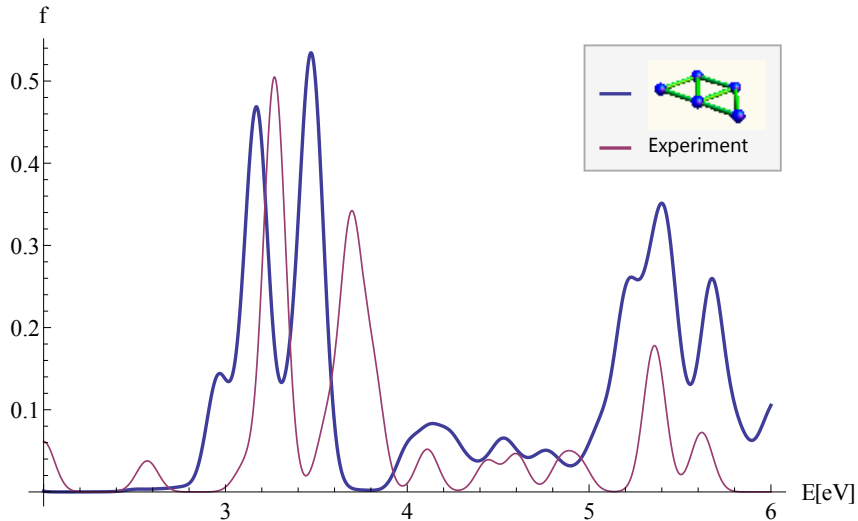


Figure 4.18: Absorption spectrum calculated for Ag_5 , the broadening factor is $\Delta = 0.06$.

has been reproduced well.

In general, there are some possible sources of errors in calculating the proper spectrum. One problem could be an incorrect equilibrium structure from the DFT calculation due to the exchange-correlation functionals, which are just approximations. Another reason for deviations in the spectra could be, that the experimental measurements were done on silver clusters embedded in a neon matrix [7].

4.3.1 Ag_3 spectrum

As two possible structures have been found for Ag_3 , the transition from one to the other structure has been studied in more detail. Some results of these efforts are shown in Figure 4.19. Spectra have been computed for different values of the parameter b , while parameter a stays fixed at $a = 2.675 \text{ \AA}$. While the spectra computed at the two structures corresponding to the two local minima differ significantly from each other, the evolution of peaks and their corresponding shifts become traceable when plotting spectra for intermedi-

4 Results

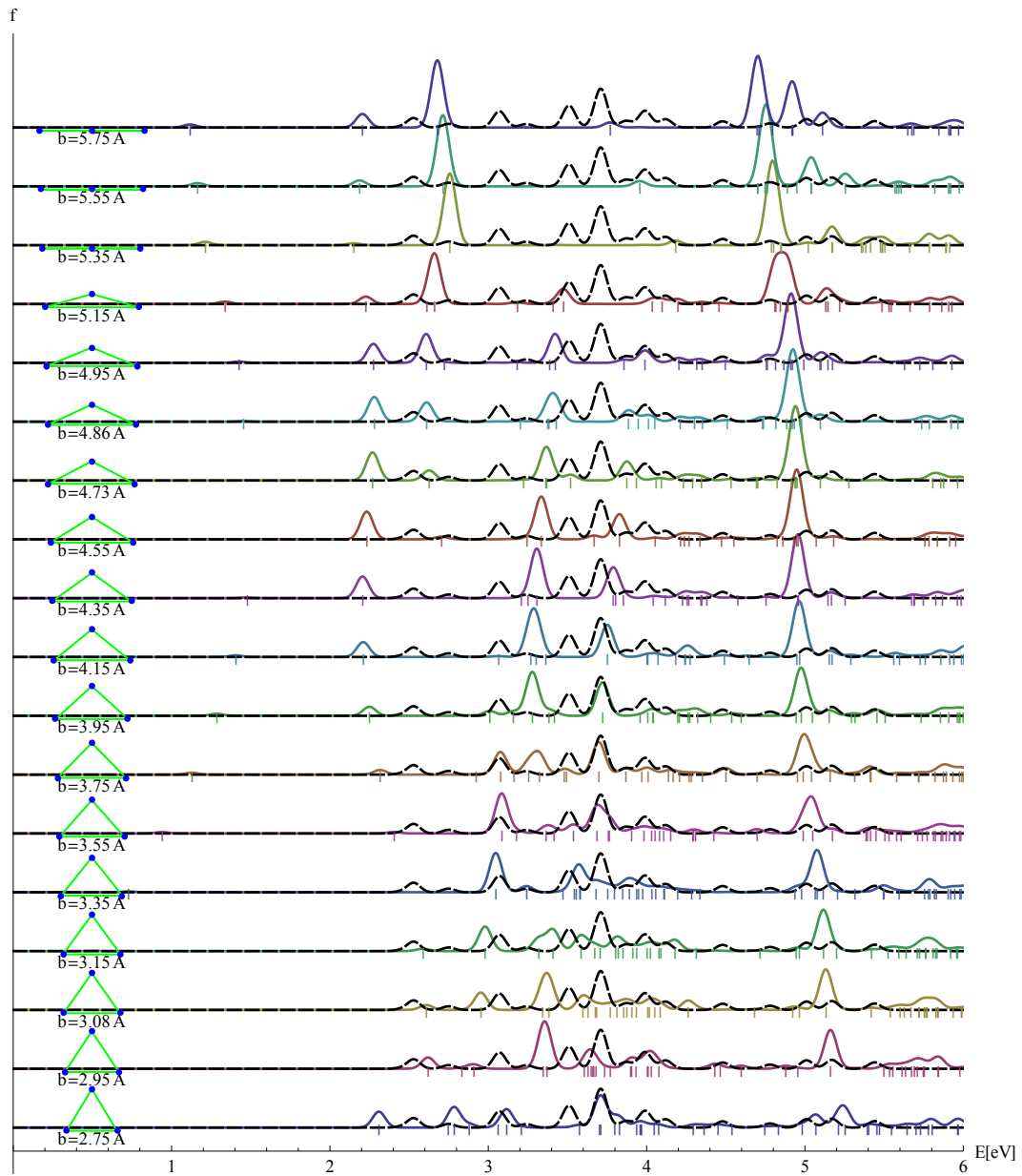


Figure 4.19: Absorption spectra calculated for Ag_3 with parameter a fixed at $a = 2.675$ Å and different values of parameter b . Comparison to experimental data plotted in black and dashed. The broadening factor for both computed and experimental data is $\Delta = 0.04$. Computed excitation energies ω_i exhibiting an oscillator strength $f_i > 0.005$ are denoted by a small vertical line |.

4 Results

ate geometries. But it is still observable, that none of the computed spectra matches the experimental data well, although some peaks do fit.

In order to analyze the nature of the optical transitions and to understand the change in the electronic structure upon altering the geometry from the triangular to the linear configuration, we plot the orbitals above and below the Fermi energy. These are referred to as highest occupied molecular orbital (HOMO) and the lowest unoccupied molecular orbital (LUMO) and their energies are plotted for spin up and spin down with corresponding orbitals for different values of b in Figure 4.20. The breaking of the bond between the two

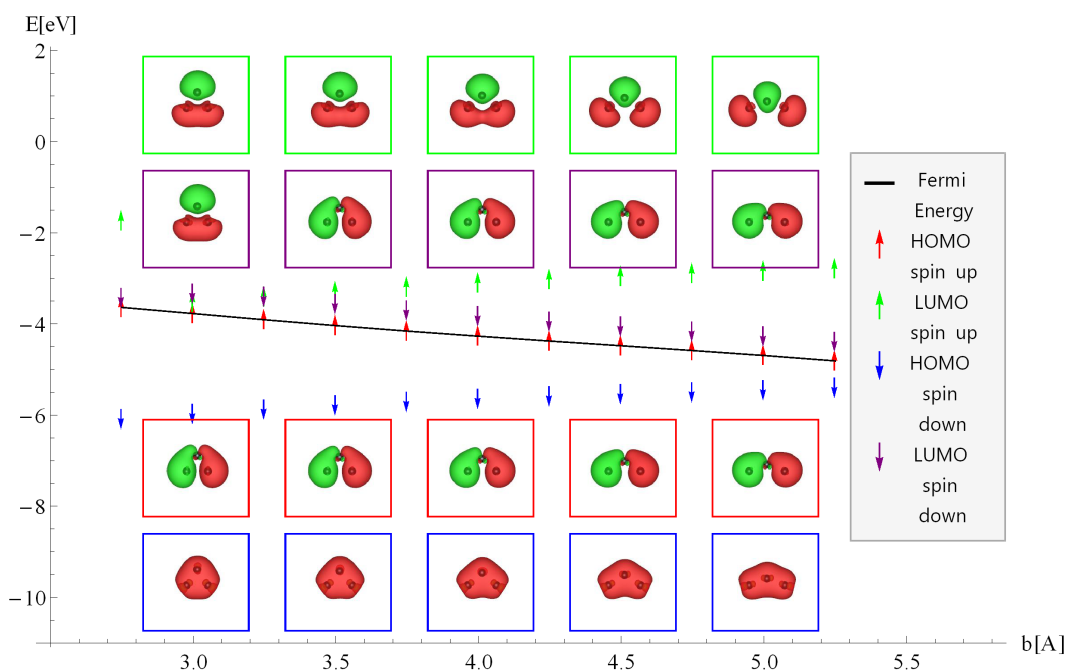


Figure 4.20: HOMO and LUMO for different Ag_3 structures with parameter a fixed at $a = 2.675 \text{ \AA}$.

atoms at the base of the triangle can be seen in this figure.

Additionally we can see, that the energy for the HOMO with spin up rises with larger values for site b and in this process reaches a energetically less favorable geometry, while the energy for the HOMO with spin down has its energetically most favorable structure at the linear configuration of Ag_3 . These two effects

4 Results

almost cancel itself and may be the reason for the low energy variation in the equilibrium potential (see i.e. Figure 4.10), although for the potential all energies below the Fermi energy have to be taken into account.

4.4 Vibronic energies for Ag_3

For the calculation of the vibronic energies of Ag_3 the trimer is modeled as three particles located on the edges of an equilateral triangle with bonds at the two sites with equal length, see Figure 4.21. To calculate vibronic energies we will consider small displacements of the atoms with respect to the equilibrium configuration. In Figure 4.9 we can observe, that the variation of the bond

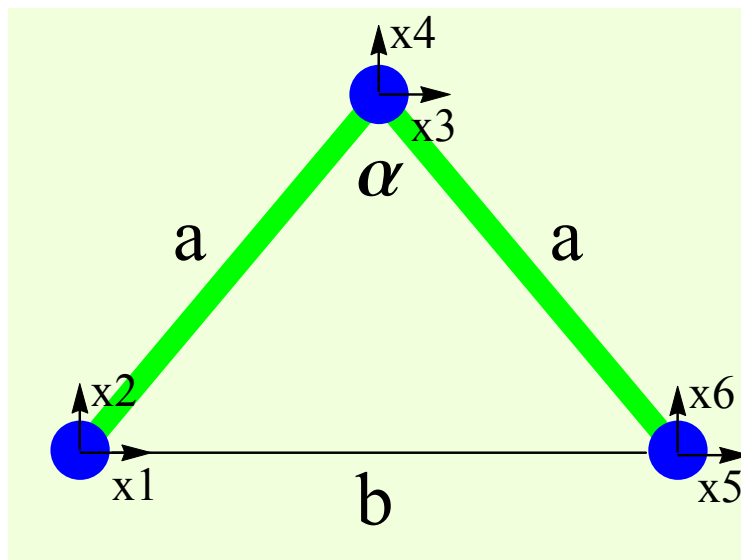


Figure 4.21: The model structure for Ag_3 with the generalized coordinate α , the angle between the two a sites, and Cartesian coordinates x_1, \dots, x_6 .

length b in the range $b = 3 - 5.5 \text{ \AA}$ leads to energy changes that correspond to a variation of bond length a in the range $a = 2.6 - 2.75 \text{ \AA}$, thus a much smaller range. From that we conclude, that the a bond is a lot more rigid compared to the b bond and we can assume, as a simplification to our problem, that changes in a and b are decoupled and can be treated separately. Because of the stiffness of the a bond we assume it to be fixed and consider the dynamics related to changes of b only. In the center of mass system this leaves us with just one degree of freedom and the generalized coordinate of choice is α , the

4 Results

angle between the two a sides. The Cartesian coordinates x_1, \dots, x_6 in Figure 4.21 can be expressed as a function of α as follows:

$$\mathbf{r} = \begin{pmatrix} x_1 \\ x_2 \\ x_3 \\ x_4 \\ x_5 \\ x_6 \end{pmatrix} = \frac{a}{3} \begin{pmatrix} -3 \sin(\alpha/2) \\ -\cos(\alpha/2) \\ 0 \\ 2 \cos(\alpha/2) \\ 3 \sin(\alpha/2) \\ -\cos(\alpha/2) \end{pmatrix} \quad (4.2)$$

To find the classical Hamiltonian of this system, we follow the instructions from Section 2.2. The Lagrangian is built from kinetic and potential energy, T and V , respectively. For the kinetic energy we find

$$T = \frac{m\dot{\mathbf{r}}^2}{2} = \frac{m}{2} \sum_{i=1}^6 \dot{x}_i^2 = \frac{ma^2}{12} (2 + \cos(\alpha)) \dot{\alpha}^2. \quad (4.3)$$

The potential energy for this problem is already known from the calculations in Section 4.2.2, and for the value $a = 2.675 \text{ \AA}$ the potential is given in Figure 4.10.

To construct the Hamiltonian H the canonical momenta from (2.8) are needed, and because V is independent of the velocities $\dot{\alpha}$ we have:

$$p_\alpha = \frac{\partial L}{\partial \dot{\alpha}} = \frac{\partial T}{\partial \dot{\alpha}} = \frac{ma^2}{6} (2 + \cos(\alpha)) \dot{\alpha} \quad (4.4)$$

The Lagrangian as a function of α and p_α then is:

$$L(\alpha, p_\alpha) = \frac{3}{ma^2} \frac{p_\alpha^2}{2 + \cos(\alpha)} - V(\alpha) \quad (4.5)$$

And according to (2.9) the classical Hamiltonian of the system reads:

$$H(\alpha, p_\alpha) = p_\alpha \dot{\alpha} - L(\alpha, p_\alpha) = \frac{3p_\alpha^2}{ma^2 (2 + \cos(\alpha))} + V(\alpha) \quad (4.6)$$

4 Results

To translate the classical Hamilton function into a Hamilton operator describing the quantum mechanical motion of the oscillations we use the prescriptions given in Equation (2.16). According to this rules the momentum has to be replaced by $p_\alpha \rightarrow -i\hbar \frac{\partial}{\partial \alpha}$. With this we obtain the time-independent Schrödinger equation:

$$\left(\frac{3}{ma^2(2 + \cos(\alpha))} \frac{\partial^2}{\partial \alpha^2} + V(\alpha) \right) \psi_v(\alpha) = E_v \psi_v(\alpha) \quad (4.7)$$

To solve the time-independent Schrödinger equation for the vibrational wave functions ψ_v we discretize the α coordinate and transfer the problem into a matrix eigenvalue equation. The grid used consists of $n = 1000$ points for α and has been solved using the method *Eigensystem* from Mathematica. The potential V_0 for the ground state has been taken from Figure 4.10 as a function of α and mirrored at π , so that $V_0(2\pi - \alpha) = V_0(\alpha) \quad \forall \pi < \alpha \leq 2\pi$. For the first electronically excited state the potential V_1 is derived from the values in Figure 4.19. These two potentials plotted as a function of α can be seen in Figure 4.22.

Additionally, Figure 4.22 shows for the ground state and the excited state potential the eigenfunctions at the corresponding eigenvalues. What is apparent at once, is, that for the excited state, the eigenfunctions are concentrated in the two deep valleys of the potential. This means, fluorescence from the first excited state to the ground state can only occur to vibronic states of the ground state, which are located beneath the two deep valleys of the excited state potential.

This qualitative finding is further emphasized by calculating the transition probabilities from a vibronic state v corresponding to the electronic ground state to a vibronic state v' at the excited state following the Franck-Condon principle. The Franck-Condon factors $\text{FC}(v', v)$ can be calculated according to Equation (2.20) using the eigenfunctions ψ_v from Equation (4.7).

The energy for the first excited electronic transition at $\omega = 0.414$ eV for the triangular equilibrium structure is then shifted to lower energies for emission and to higher energies for absorption. The results of these shifts are plotted in

4 Results

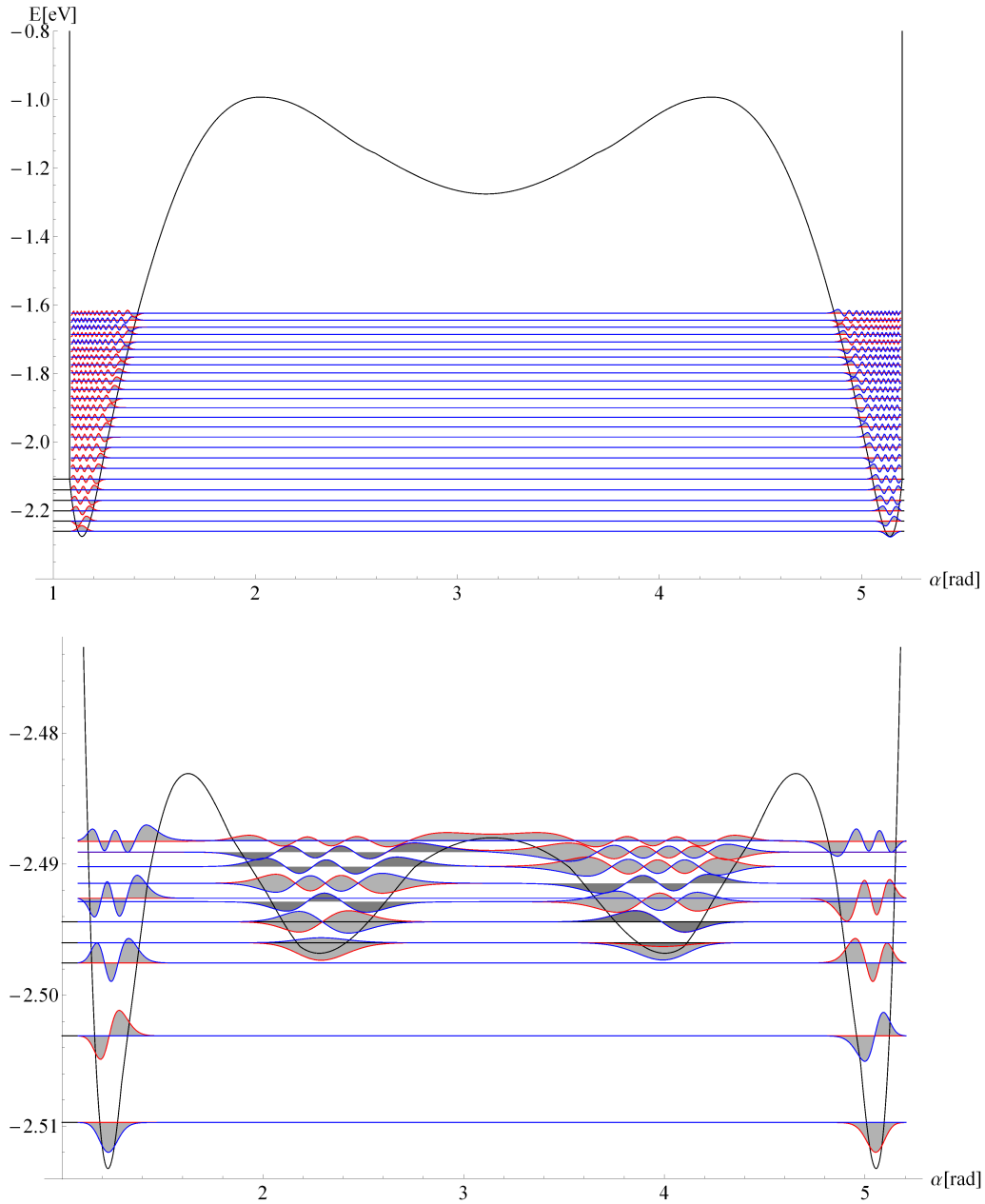


Figure 4.22: Potential of ground state and the first excited state mirrored at π with the first 22 and 50 eigenvectors, respectively. The eigenfunctions for the paired eigenvalues are colored red and blue alternately.

4 Results

Figure 4.23, the discrete peaks are broadened with the Gaussian function from (4.1). It can be seen, that the Franck-Condon factors are non-zero not only

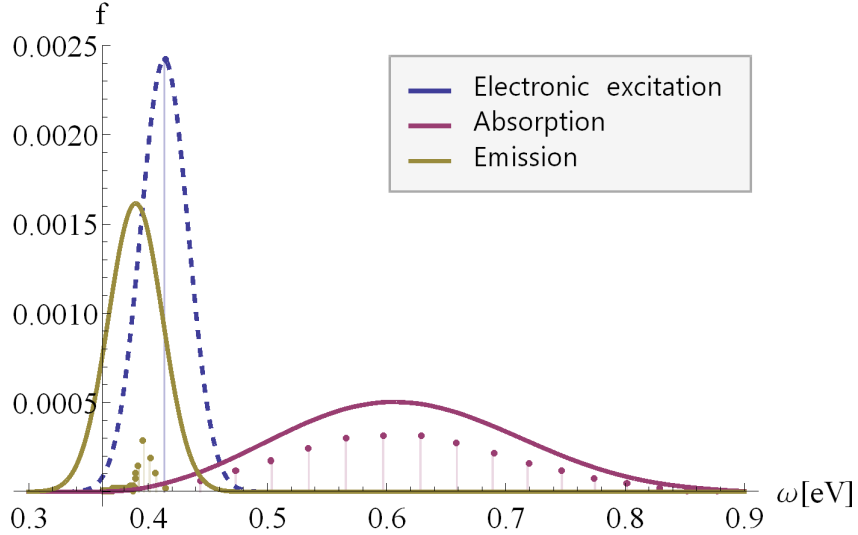


Figure 4.23: Franck-Condon factors calculated for eigenfunctions in Figure 4.22 are denoted by dots, the broadening factor is $\Delta = 0.02$ eV.

for one vibronic transition, but for a series of transitions. So the overall peak position of the transition, gets shifted and the oscillator strength is distributed to several vibronic transitions according to those factors.

Because the eigenvalues of the ground state are very close together (see Figure 4.22), within the range of $k_B T$, at finite temperature we must take into account, that not only the ground state of the vibronic states is occupied but also excited states. To this end, the Boltzmann statistics can be used. The probability p_i for the occupation of a higher lying state with energy E_i is given as [32]

$$p_i(T) = \frac{1}{Z} \exp^{-\frac{E_0 - E_i}{k_B T}}, \quad (4.8)$$

with Z being the partition function and k_B the Boltzmann constant. The Franck-Condon factors are now additionally weighted with the occupation probability for different temperatures. In Figure 4.24 the shifted peaks are plotted for various temperatures. We see, that the emission spectrum does not

4 Results

vary much with an increase of temperature, which has to be since $k_B T$ is much smaller than the energy differences of the eigenvalues of the excited state. This

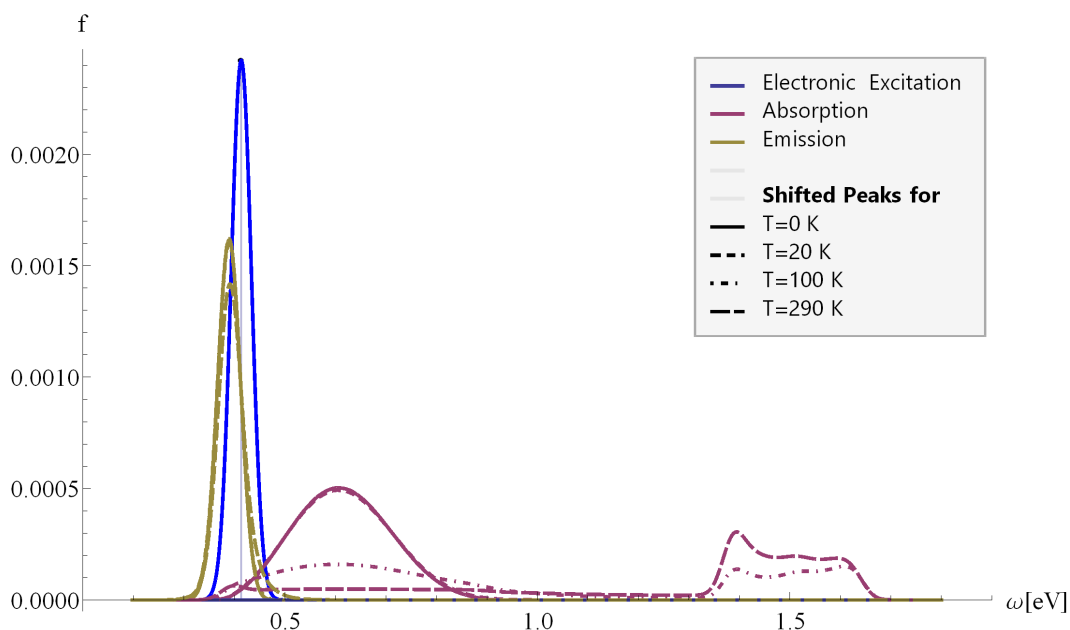


Figure 4.24: Plot of electronic excitation at $\omega = 0.414$ eV and the shifted excitations due to vibronic transitions for absorption and emission with a broadening factor of $\Delta = 0.02$ for different temperatures.

is different with the absorption spectra. While for $T = 0$ K and for $T = 20$ K the spectra are almost the same, a larger shift of about 1 eV of the absorption to higher energies can be observed for $T = 100$ K and $T = 290$ K. This is a result of the occupation of eigenstates, whose eigenfunctions are centered in the ground state potential in Figure 4.22 and have a significantly larger overlap to eigenfunctions of higher lying eigenstates of the excited potential. In Figure 4.22 it can also be seen, that the first eigenfunctions, which are centered in the excited potential, have eigenvalues about 1 eV higher than the ground state eigenvalue of the excited potential. This corresponds to the shift of the absorption spectra observable in Figure 4.24.

5 Conclusion

In this paper we investigated the structure and absorption spectra of small silver clusters within DFT and TDDFT. The calculated absorption spectra showed an overall good agreement with experimental data from literature.

We particularly focussed on Ag_3 , which exhibited two equilibrium configurations, one being a nearly linear and the other a triangular structure. For those two structures, and for the evolution from one to the other, we computed the absorption spectra. For this changing of the configuration a shift of the peaks could be observed. Also we studied the breaking of the bond at the base of the triangular structure for the evolution to the linear configuration at the orbitals of the bands at the Fermi energy (HOMO and LUMO).

Additionally we investigated vibronic transitions for Ag_3 , their influence on an electronic transition, and the effect of a temperature $T > 0$ K. As suspected, the inclusion of the vibronic transitions displaced the electronic peak to higher energies for absorption and to lower energies for emission. For high temperatures (100 – 290 K) we observed a shift of the absorption peaks to even higher energies, while the peaks for the emission did not significantly change.

Within this work we did only look upon the vibronic transitions for the first electronic peak, which got shifted significantly for higher temperatures. So to get a spectrum that better matches experimental data, it may be necessary to look upon the vibronic transitions for the main electronic peaks in the spectrum. In addition, further investigations of the influence of temperature on the spectrum could be a way to improve the calculated spectra.

Acknowledgements

First, I want to thank my wife for her love and encouragement and for not getting annoyed with my constant asking for vocabulary advice. I am also so glad my little daughter always welcomes me so gushingly when I come home and cheering me up with her smile.

I want to thank my supervisors, Prof. Peter Puschnig and Prof. Ulrich Hohenester, for their advice and supervision and for offering me the possibility to work in this interesting field of physics.

I also would like to thank my parents, for giving me the opportunity to study in the first place, for their ongoing support and for always being interested in what I am occupied with at the moment.

Used Software

- **ABINIT**
Version: 6.12,
Website: <http://www.abinit.org/downloads/source-packages/>,
date: 15.01.2013.
- **TEXnicCenter**
Version: 1.0,
Website: <http://www.texniccenter.org/resources/downloads/29>,
date: 15.01.2013.
- **VESTA**
Version: 3.1.0,
Website: <http://jp-minerals.org/vesta/en/download.html>,
date: 15.01.2013.
- **Wolfram Mathematica**
Version: 9.0.0.0,
Website: <http://www.wolfram.com/solutions/education/students>,
date: 15.01.2013.

Bibliography

- [1] Andrew P. Bartko Lynn A. Peyser, Amy E. Vinson and Robert M. Dickson. Photoactivated fluorescence from individual silver nanoclusters. *Science*, 291, 2001. [1.1](#), [1](#)
- [2] Juan C Idrobo and Serdar Ögüt. Size dependence of the static polarizabilities and absorption spectra of ag. *Physical Review B*, 72, 2005. [1](#), [4](#), [4.2](#), [4.2.3](#), [4.3](#), [4.2.3](#), [4.13](#)
- [3] Jiri Pittner Vlasta Bonacic-Koutecky and Marc Boiron. An accurate relativistic effective core potential for excited states of ag atom. *Journal of Chemical Physics*, 110, 1998. [1](#), [4](#), [4.2.3](#), [4.3](#), [4.13](#)
- [4] Murilo L. Tiago, Juan C. Idrobo, Serdar Ögüt, Julius Jellinek, and James R. Chelikowsky. Electronic and optical excitations in agn clusters (n=1–8): Comparison of density-functional and many-body theories. *Physical Review B*, 79, 2009. [1](#), [4](#)
- [5] M. Harb, F. Rabilloud, D. Dimon, A. Rydlo, S. Lecoultre, F. Conus, V. Rodrigues, and C. Felix. Optical absorption of small silver clusters: Agn, (=4–22). *Journal of Chemical Physics*, 129, 2008. [1](#)
- [6] Rene Fournier. Theoretical study of the structure of silver clusters. *Journal of Chemical Physics*, 115, 2001. [1](#), [4](#), [4.2.3](#), [4.3](#)
- [7] S. Lecoultre, A. Rydlo, J. Buttet, C. Félix, S. Gilb, and W. Harbich. Ultraviolet-visible absorption of small silver clusters in neon: Ag[sub n] (n = 1–9). *The Journal of Chemical Physics*, 134(18):184504, 2011. [1](#), [4](#), [4.3](#), [4.3](#)
- [8] S. Fedrigo, W. Harbich, and J. Buttet. Optical response of Ag₂, Ag₃, Au₂, and Au₃ in argon matrices. *J. Chem. Phys.*, 99(8), October 1993. [1](#)

Bibliography

- [9] W. Harbich, S. Fedrigo, and J. Buttet. The optical absorption spectra of small silver clusters ($n = 5-11$) embedded in argon matrices. *Chemical Physics Letters*, 195, July 1992. [1](#)
- [10] V. Beutel, H.-G. Kramer, G. L. Bhale, M. Kuhn, K. Weyers, and W. Demtroder. High-resolution isotope selective laser spectroscopy of Ag_2 molecules. *The Journal of Chemical Physics*, 98(4):2699–2708, 1993. [1](#), [4.2.3](#), [4.3](#)
- [11] W. Demtröder. *Experimentalphysik 3: Atome, Moleküle und Festkörper*. Experimentalphysik / Wolfgang Demtröder. Springer, 2005. [2.1](#), [2.4](#)
- [12] T. Fließbach. *Mechanik: Lehrbuch Zur Theoretischen Physik I*. Spektrum Akademischer Verlag GmbH, 4 edition, 2003. [2.2.1](#), [2.2.2](#), [2.2.2](#)
- [13] L. D Landau and E. M Lifshits. *Mechanics*. Butterworth-Heinemann, Oxford, 3 edition, 2000. [2.2.1](#)
- [14] Herbert Goldstein, Charles P. Poole, and John L. Safko. *Classical Mechanics (3rd Edition)*. Addison-Wesley, 3 edition, 2001. [2.2.1](#), [2.2.2](#)
- [15] T. Fließbach. *Quantenmechanik: Lehrbuch Zur Theoretischen Physik III*. BI-Wiss.-Verlag, 1991. [2.3](#), [2.3](#)
- [16] F. Schwabl. *Quantenmechanik (QM I)*:. Springer-Lehrbuch. Springer, 2004. [2.3](#)
- [17] P.W. Atkins and R.S. Friedman. *Molecular Quantum Mechanics*. Oxford University Press, 4 edition, 2008. [2.1](#), [2.4](#)
- [18] W Kohn. Nobel lecture: Electronic structure of matter—wave functions and density functionals. *Reviews of Modern Physics*, 1999. [3](#), [3.1](#), [3.1](#), [3.1](#), [3.1](#), [3.1](#)
- [19] David S. Sholl. *Density Functional Theory*. John Wiley & Sons, Inc., 2009. [3.1](#), [3.1](#)

Bibliography

- [20] W. Kohn and L. J. Sham. Self-consistent equations including exchange and correlation effects. *Phys. Rev.*, 140(4A):A1133–A1138, Nov 1965. [3.1](#), [3.1](#)
- [21] P. Hohenberg and W. Kohn. Inhomogeneous Electron Gas. *Physical Review*, 136:864–871, November 1964. [3.1](#), [3.1](#)
- [22] D. M. Ceperly and B. J. Alder. Ground state of the electron gas by a stochastic method. *Phys. Rev. Lett.*, 45:566, 1980. [3.1](#), [3.1](#)
- [23] J. P. Perdew, K. Burke, and M. Ernzerhof. Generalized Gradient Approximation Made Simple. *Phys. Rev. Lett.*, 77:3865, 1996. [3.1](#), [4](#)
- [24] Erich Runge and E. K. U. Gross. Density-functional theory for time-dependent systems. *Physical Review Letters*, 52:997–1000, 1984. [3.2](#)
- [25] M. E. Casida. *Time-Dependent Density Functional Response Theory for Molecules*, chapter 5, page p. 155. Singapore, World Scientific, 1995. [3.2](#), [3.2.1](#), [3.2.1](#)
- [26] Mark E. Casida, Kim C. Casida, and Dennis R. Salahub. Excited-state potential energy curves from time-dependent density-functional theory: A cross section of formaldehyde’s 1a 1 manifold. *Int. J. Quant. Chem.*, 70:933–941, 1998. [3.2](#), [3.2.1](#)
- [27] M. E. Casida, Christine Jamorski, Kim C Casida, and Dennis R Salahub. Molecular excitation energies to high-lying bound states from time-dependent density-functional response theory: Characterization and correction of the time-dependent local density approximation ionization threshold. *The Journal of Chemical Physics*, 108(11):4439, 1998. [3.2](#)
- [28] Serdar Ögüt Igor Vasiliev and James R. Chelikowsky. Ab initio excitation spectra and collective electronic response in atoms and clusters. *Physical Review Letters*, 82, 1999. [3.2.1](#)
- [29] X. Gonze, B. Amadon, P.-M. Anglade, J.-M. Beuken, F. Bottin, P. Boulanger, F. Bruneval, D. Caliste, R. Caracas, M. Côté, T. Deutsch,

Bibliography

- L. Genovese, P. Ghosez, M. Giantomassi, S. Goedecker, D. R. Hamann, P. Hermet, F. Jollet, G. Jomard, S. Leroux, M. Mancini, S. Mazevet, M. J. T. Oliveira, G. Onida, Y. Pouillon, T. Rangel, G.-M. Rignanese, D. Sangalli, R. Shaltaf, M. Torrent, M. J. Verstraete, G. Zerah, and J. W. Zwanziger. ABINIT: First-principles approach to material and nanosystem properties. *Computer Physics Communications*, 180:2582–2615, December 2009. [4](#)
- [30] J. P. Perdew and Y. Wang. Accurate and simple analytic representation of the electron-gas correlation energy. *Phys. Rev. B*, 45:13244–9, 1992. [4](#)
- [31] C. Fiolhais, F. Nogueira, and M.A.L. Marques. *A Primer in Density Functional Theory*. Lecture Notes in Physics. Springer, 2003. [4.2.2](#)
- [32] T. Fließbach. *Statistische Physik: Lehrbuch Zur Theoretischen Physik IV*. Spektrum Akademischer Verlag GmbH, 4 edition, 2007. [4.4](#)